Rochester Institute of Technology
RIT Scholar Works

Theses

3-1-1999

Experimental investigation of electromechanical surface damping

Rolf Fisher Orsagh

Follow this and additional works at: https://scholarworks.rit.edu/theses

Recommended Citation
Orsagh, Rolf Fisher, "Experimental investigation of electromechanical surface damping" (1999). Thesis. Rochester Institute of Technology. Accessed from

This Thesis is brought to you for free and open access by RIT Scholar Works. It has been accepted for inclusion in Theses by an authorized administrator of RIT Scholar Works. For more information, please contact ritscholarworks@rit.edu.

Experimental Investigation of Electromechanical Surface Damping

by Rolf Fisher Orsagh

A thesis submitted in partial fulfillment
of the requirements for the degree of

Master of Science
in
Mechanical Engineering

Approved by: Professor _____
Dr. Hany Ghoneim, Thesis Advisor

Professor _____
Dr. Kevin Kochersberger, Committee Member

Professor _____
Dr. Wayne Walter, Committee Member

Professor _____
Dr. Charles Haines, Department Head

Department of Mechanical Engineering
College of Engineering
Rochester Institute of Technology

March 1999

Permission to Reproduce

Thesis Title: "Experimental Investigation of Electromechanical Surface Damping"

I, Rolf Orsagh, hereby grant permission to the Wallace Memorial Library of the Rochester Institute of Technology to reproduce my thesis in whole or in part. Any reproduction can not be used for commercial use or profit.

March 1999

Contents

Figures ii
Acknowledgements iii
Abstract iv
Introduction 1
  Literature Review 2
    Constrained Layer Damping 2
    Active Control with Piezoelectric Materials 3
    Active Constrained Layer Damping 3
    Resonant Shunting of Piezoelectric Elements 4
  Problem Statement 10
Theory 11
  Viscoelastic Materials 11
  Piezoelectric Materials 15
Experimental Work 16
Results and Discussion 22
Conclusion 35
References 36
Appendix A 37
Appendix B 41
Appendix C 42
Appendix D 45

Figures

Figure 1 a) Undeformed constrained layer treatment b) Deformed constrained layer treatment 2
Figure 2 Active constrained layer damping increases the shear angle in the viscoelastic material. 4
Figure 3 Effect of a resonantly shunted piezoelectric element on the FRF of the host structure 6
Figure 4 Synthetic inductor 7
Figure 5 Effect of varying the damping resistance in a resonant shunt 9
Figure 6 Three-parameter model of a viscoelastic material 11
Figure 7 Modulus of a generic 3 parameter model 13
Figure 8 Loss factor of a generic 3 parameter model 14
Figure 9 Schematic diagram of a piezoelectric element 15
Figure 10 Diagram of a beam treated with the EMSD 17
Figure 11 Experimental apparatus 19
Figure 12 Piezoelectric elements and shunt 20
Figure 13 The second resonance peak at 55°C of the beam treated with DYAD 609 23
Figure 14 The second resonance peak at 25°C of the beam treated with DYAD 609 23
Figure 15 The second resonance peak at 25°C of the beam treated with DYAD 606 24
Figure 16 The third resonance peak at 25°C of the beam treated with DYAD 606 24
Figure 17 DYAD 609 mode 2 temperature summary 26
Figure 18 DYAD 609 mode 3 temperature summary 27
Figure 19 DYAD 606 mode 2 temperature summary 29
Figure 20 DYAD 606 mode 3 temperature summary 30
Figure 21 Effectiveness of the constrained layer and EMSD as functions of frequency 31
Figure 22 Dr. Ghoneim's FEM results (DYAD 606 at 25°C) 33
Figure 23 Experimental results (DYAD 606 at 25°C) 33
Figure 24 Negative impedance converter 38
Figure 25 The synthetic inductor is composed of two negative impedance converters. 39
Figure 26 Modulus and loss factor of DYAD 606. © SoundCoat, Inc. 41
Figure 27 Modulus and loss factor of DYAD 609. © SoundCoat, Inc. 41
Figure 28 Diagram of the linear bearing and beam with accelerometers 42
Figure 29 Frequency response function showing the bearing effect (Tail/Reference) 44
Figure 30 Linearity verification for mode 2 of the untreated beam 46
Figure 31 Linearity verification for mode 3 of the untreated beam 46
Figure 32 Linearity verification for mode 2 of the treated beams 47
Figure 33 Linearity verification for mode 3 of the treated beams 47

Acknowledgements

The completion of this thesis would not have been possible without support and assistance from many people. I am grateful to everyone who contributed to this project. My wife Cynthia gave me many helpful suggestions, encouragement, and her patience. Dr. Ghoneim, my advisor, guided me through many difficulties and taught me so much. Dr. Kochersberger shared his experimental expertise and humor with me. Dr. Walter and Dr. Budynas provided constructive criticism. Dave Hathaway, Jim Greanier, and Tom Locke assisted me in building the experimental apparatus. Dr. Jim Wu shared his experience with resonant shunts. Dr. Palmer, Dr. Mukund, and Dr. Titus assisted me with their knowledge of electronics. Dr. Goodwin and Bill Colaiaco made an environmentally controlled chamber available.

Abstract

Electromechanical Surface Damping (EMSD) is a hybrid technique that incorporates constrained layer damping (CLD) and shunted piezoelectric element methods for the suppression of vibration in light beam-like or plate-like structures. The EMSD technique enhances the damping effectiveness (peak amplitude suppression) at targeted resonant frequencies, and may therefore be used to extend the damping effectiveness of the constrained layer damping technique over a broader temperature and frequency range than CLD alone. This performance enhancement was demonstrated experimentally by comparing the steady state frequency response of cantilever beams that were partially treated with the CLD and EMSD techniques. The experimental results also agreed with the results of a corresponding finite element model.

Introduction

Vibration control has played an increasingly important role in improving the performance and durability of modern machinery. For example, vibration damping treatments have been used to improve the performance of automobile brakes by preventing squeal[1]. Damping treatments have also been used to reduce vibration-induced fatigue in military aircraft[2]. In the automotive and aerospace industries, there is a demand for lightweight damping treatments.

The condition of resonance is of great importance in vibration control. Resonance occurs when a structure is excited at one of its natural frequencies. The amplitude of vibration at resonance can be orders of magnitude larger than the quasi-static response to the same level of excitation. For linear systems, the amplitude of vibration at resonance is only limited by damping. When a condition of resonance exists, the amplitude of vibration can generally be reduced in two ways: First, the excitation frequency or the natural frequency can be changed to avoid resonance. Unfortunately, it is often difficult to avoid resonance. Second, damping can be added to the system to reduce the response at resonance.

New damping techniques have emerged in response to the need for vibration control. Two materials, viscoelastics and piezoelectrics, have been used in a variety of new damping techniques. The popularity of these materials may be attributed in part to the fact that they can produce high damping to weight ratios and they are well suited to controlling the vibration of beam-like and plate-like structures. Both of these characteristics are important to the automotive and aerospace industries.

Literature Review

Constrained Layer Damping

Constrained layer damping was proposed in 1959 by Kerwin[3] for damping vibration in beam and plate-like structures. Today, constrained layer damping is widely used to control vibration in ships, aircraft, and other machinery[4]. Constrained layer damping treatments are simple, completely passive, and therefore very reliable.

A Constrained layer damping treatment consists of a sheet of viscoelastic material bonded between the surface of the structure to be damped and a stiff cap (the constraining layer) as shown in figure 1a. Bending of the structure during vibration produces shear in the viscoelastic material as shown in figure 1b. While an unconstrained viscoelastic layer would dissipate vibration energy, the constraining layer significantly improves the damping effectiveness by increasing the shear angle (γ).

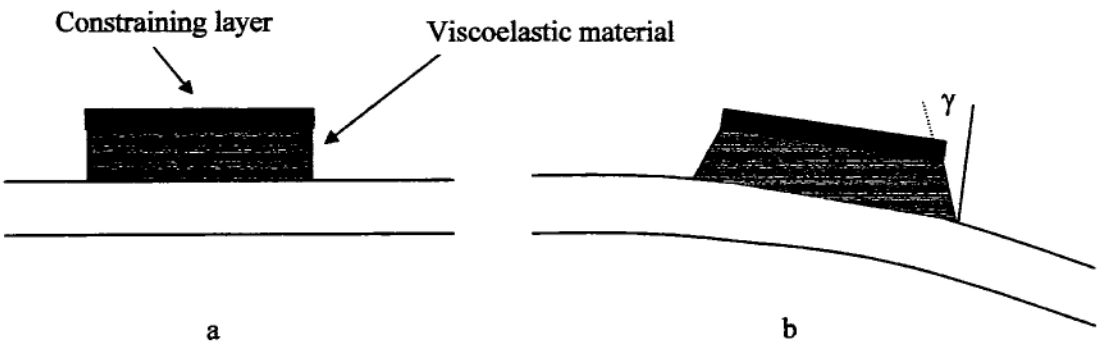

Figure 1 a) Undeformed constrained layer treatment b) Deformed constrained layer treatment

The most significant limitation of constrained layer damping treatments is their lack of adaptability. Constrained layer damping treatments must be designed for a specific temperature and frequency of vibration because the damping properties of viscoelastic materials depend on these quantities. Damping effectiveness is lost when these conditions change. A more robust

constrained layer damping treatment can be constructed by layering different viscoelastic materials, but doing so significantly increases the weight of the damping treatment[5].

Active Control with Piezoelectric Materials

Piezoelectric elements have been used alone as both actuators and sensors with active control[2]. The piezoelectric element is bonded directly to the surface of the structure to be damped. A controller uses the signal from a sensor to drive a piezoelectric element and suppress vibration in the structure. While this technique is highly effective, it requires a complex controller and can become unstable under off design conditions.

Active Constrained Layer Damping

Many studies have explored the use of viscoelastic and piezoelectric materials together. The most popular technique, active constrained layer damping[5,6] replaces the constraining layer with a piezoelectric element under active control.

The piezoelectric element enhances the damping provided by the constrained layer by increasing the shear angle in the viscoelastic material as shown in figure 2. The supplemental damping can therefore extend the effectiveness of constrained layer damping over a broader temperature and frequency range.

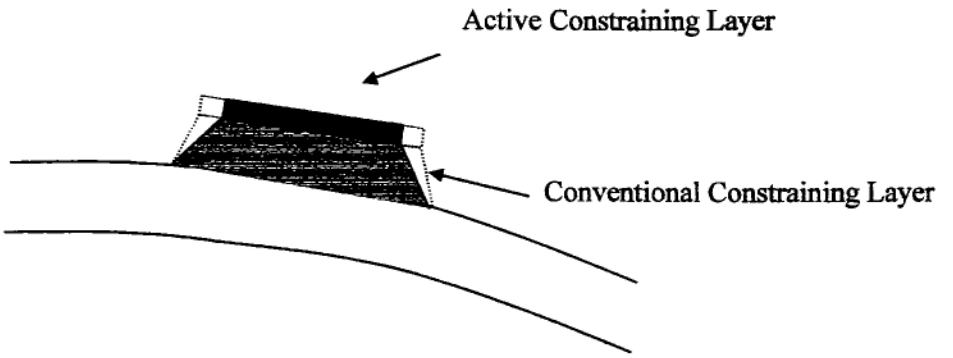

Figure 2 Active constrained layer damping increases the shear angle in the viscoelastic material

Active constrained layer damping is also less prone to instability than direct use of an actively controlled piezoelectric element. However, active constrained layer damping inherits the disadvantage of complexity from its reliance on active control.

Resonant Shunting of Piezoelectric Elements

A passive damping treatment can be constructed by shunting a piezoelectric element with a simple passive electronic circuit. Mechanical energy is converted to electrical energy by the piezoelectric element and then the electrical energy is dissipated through a resistor in the shunt as heat. Hagwood and von Flotow[7] have shown that the resistively shunted piezoelectric element can usually provide more damping than a viscoelastic damper of the same weight. Furthermore, the damping properties of shunted piezoelectric elements depend far less on temperature than those of viscoelastic materials[7].

Hagwood and von Flotow showed that damping effectiveness can be increased by several orders of magnitude over a narrow frequency range by adding an inductor to the shunt. The inductor (L) and the capacitance (C) of the piezoelectric element act together to form a resonant (LC) circuit

with a natural frequency (f) given by equation 1. The electrical circuit is essentially an additional degree of freedom on the system similar to a dynamic vibration absorber to which damping has been added.

$$f = \frac{1}{2\pi\sqrt{LC}} \tag{1}$$

When the resonant circuit is tuned to a natural frequency of the mechanical system, the structural resonance peak is split by an anti-resonance as shown in figure 3. The FRF in figure 3 was generated experimentally by reproducing the resonant shunting experiment conducted by Hagwood and von Flotow. A piezoelectric element was bonded directly to a beam and the FRF was measured with and without the shunt attached. The anti-resonance is relatively shallow due to the internal resistance of the inductor. The required inductance of the shunt can be approximated from the capacitance of the piezoelectric elements and the resonant frequency usimg equation 1. For example, if the piezoelectric elements have a combined capacitance of 14.2 nF and the resonant frequency is 225 Hz, then the inductance of the shunt must be roughly 35 H.

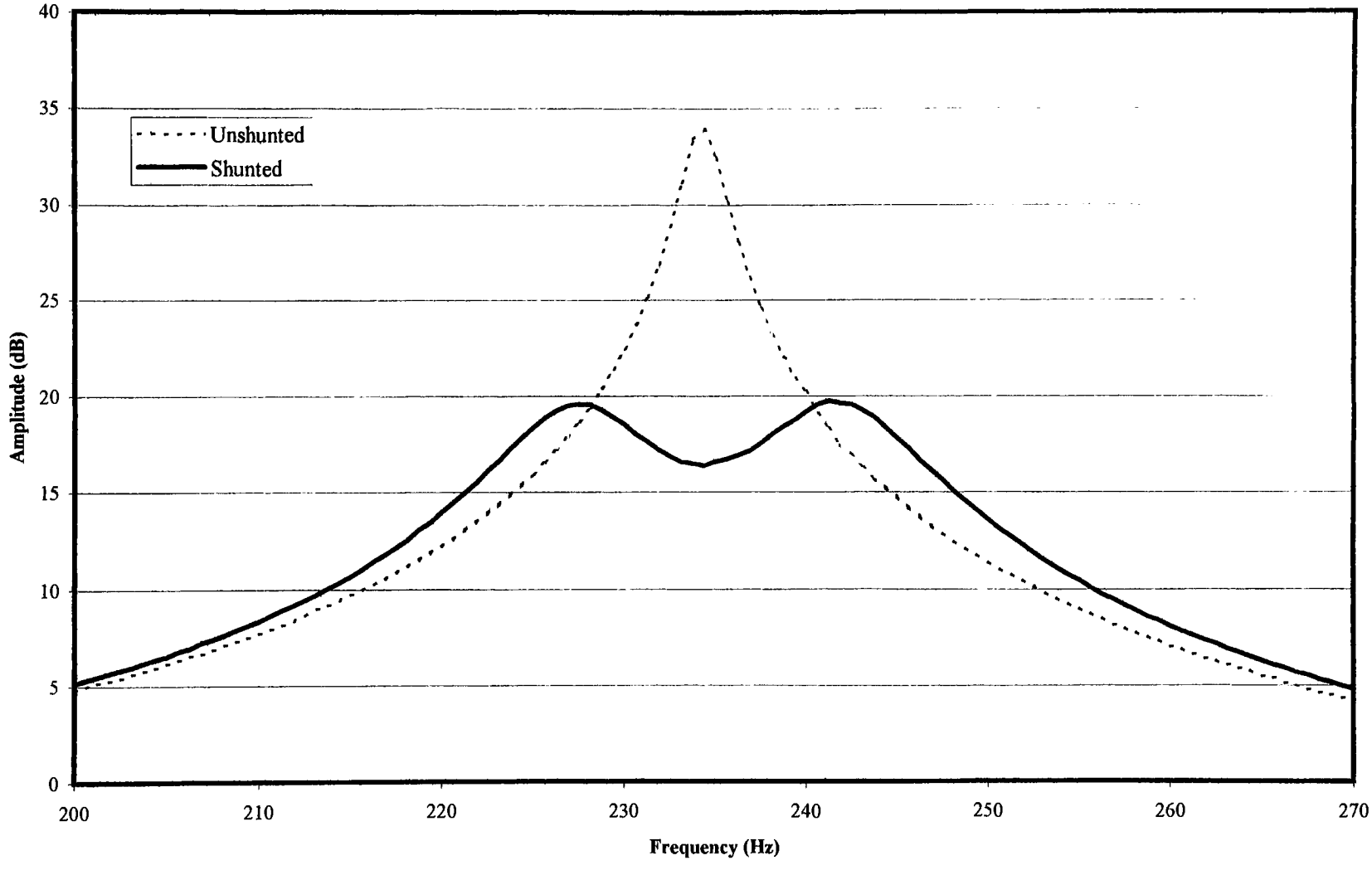

Figure 3 Effect of a resonantly shunted piezoelectric element on the FRF of host structure

Two problems arise with inductors of the size often required for resonant shunting of piezoelectric elements. First, the weight of the inductor may be too large for many applications[7]. Second, the internal resistance of the inductor may exceed the optimum damping resistance. Fortunately, a group at McDonnell Douglas[8] developed a synthetic inductor as shown in figure 4 that is smaller and has less internal resistance than large conventional inductors.

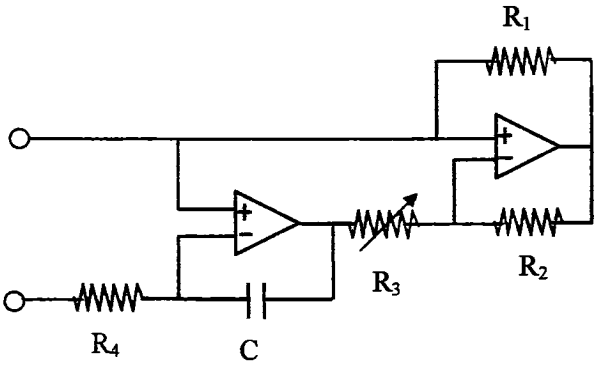

Figure 4 Synthetic inductor

An equation for inductance of the synthetic inductor is derived in Appendix A and the result is stated in equation 2. This equation only applies when the voltage across the inductor is less than the supply voltage to the op-amps. A significant advantage of the synthetic inductor over a conventional counterpart is the ease with which the inductance can be changed. The inductance of the synthetic inductor can be adjusted with the potentiometer, R_3.

$$L = \frac{R_1 R_3 R_4 C}{R_2} \tag{2}$$

Electrical damping can be supplied by the resistor either in series or in parallel with the inductor. A parallel connection was shown superior by Wu[9] because it eliminates the need for iterative

tuning. The optimum damping resistance can be determined from the resonance peak. Figure 5 shows the effect of varying a damping resistance that is in parallel with the inductor. The FRF in figure 5 was generated by reproducing the resonant shunting experiment conducted by Hagwood and von Flotow[3]. The optimization criteria used by Hagwood and von Flotow equated the amplitude of the response at the tuned frequency with that at the points S and T. The resonance peak must therefore appear flat between points S and T.

A resonantly shunted piezoelectric element can damp vibration over a broad range of temperatures, but it is only effective at the resonant frequency of the shunt. While it is possible to retune the shunt to accommodate changing system parameters, a more robust system would be preferable.

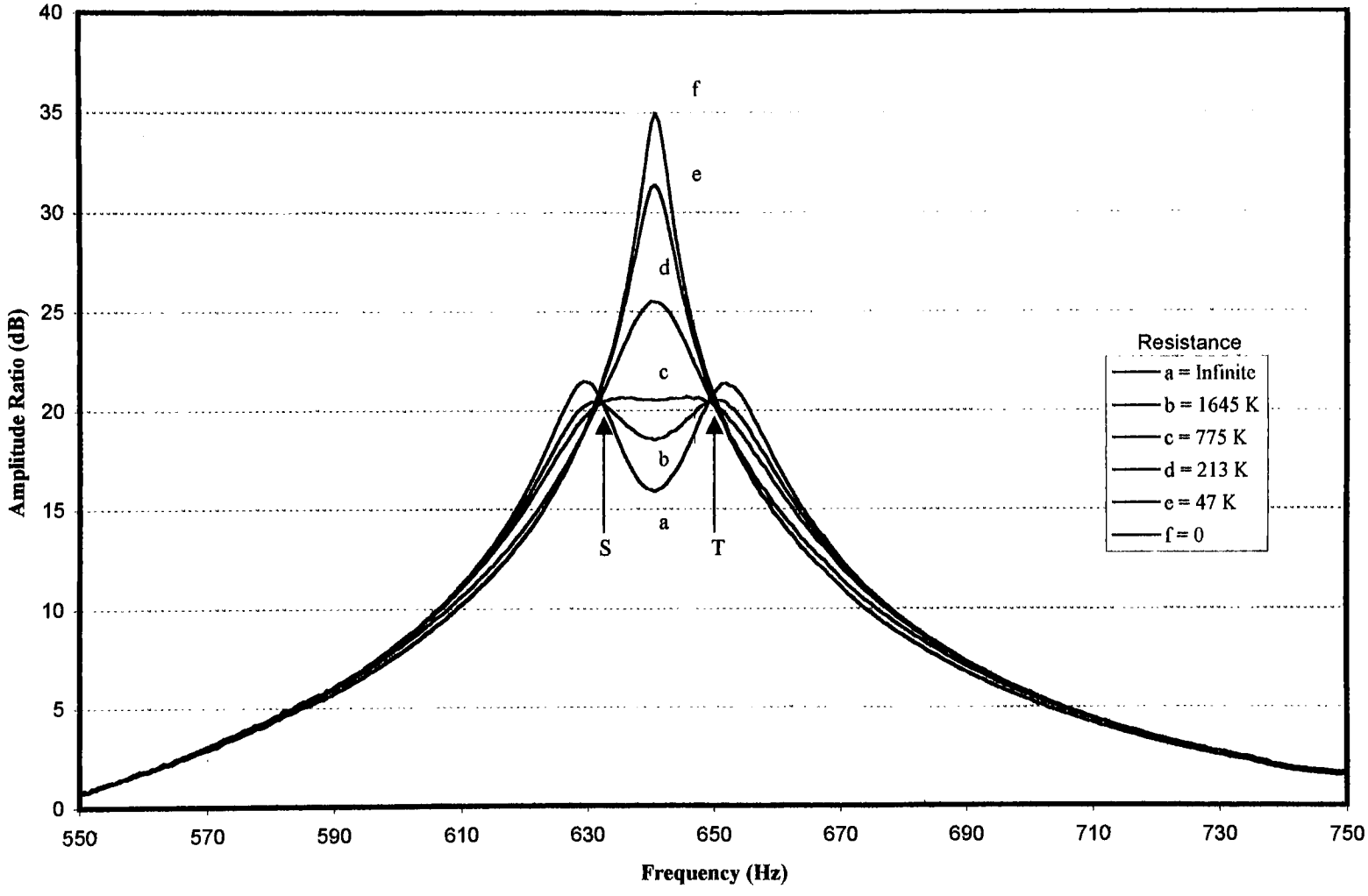

Figure 5 Effect of varying the damping resistance in a resonant shunt

Problem Statement

A completely passive combination of viscoelastic and piezoelectric materials, called electromechanical surface damping (EMSD) was proposed by Ghoneim[10]. The EMSD technique is similar to active constrained layer damping, except that the piezoelectric element is shunted with a passive resonant circuit. As with active constrained layer damping, the EMSD technique augments the damping from the constrained layer by dissipating energy electrically. As with conventional resonant shunting of piezoelectric elements, the piezoelectric element couples the mechanical system with a damped electrical circuit that is tuned to one of the structural natural frequencies. The amount of electrical damping can be adjusted to optimize the effectiveness of the damping treatment.

The EMSD technique overcomes many of the disadvantages of active constrained layer damping and resonantly shunted piezoelectric elements. EMSD is simpler than active constrained layer damping because EMSD does not require a complicated control circuit. The EMSD technique utilizes an electrical shunt that is much simpler and less prone to instability than active control circuits. The EMSD is more robust than resonantly shunted piezoelectric elements because constrained viscoelastic layer continues to provide damping if the shunt is not properly tuned or if the shunt fails.

The theoretical portion of Ghoneim's research predicted that the EMSD technique would extend the effectiveness of the constrained layer damping treatment over a broader temperature and frequency range. Unfortunately, the experimental portion of his study was inconclusive[11]. The objective of this research is to experimentally demonstrate the ability of EMSD to enhance the performance of a constrained layer damping treatment. The experiment will be consistent with Ghoneim's model of a cantilever treated with the EMSD.

Theory

Viscoelastic Materials

A class of polymers called viscoelastic materials is widely used for vibration control. Viscoelastic materials behave in a manner similar to viscous liquids in that they dissipate energy by internal friction when they are deformed. However, unlike viscous liquids, viscoelastic materials do not experience permanent deformation unless they are stressed beyond their yield point[4].

The elastic and dissipative properties of viscoelastic materials are produced by the tangled polymer chains of which they are composed. When the material is deformed, the chains stretch and rub against one another. Deformation energy is dissipated as heat from friction between the chains as they rub together. Deformation energy is also stored as potential energy when bonds between the tangled chain loops stretch. Once the load is removed, the bonds contract and cause the material to regain its original shape[4].

When stress is applied to a viscoelastic material, the strain depends both on the magnitude of the stress and on time. A simple model of viscoelastic materials, called the three-parameter model, can be constructed from two springs and a dashpot as shown in figure 6.

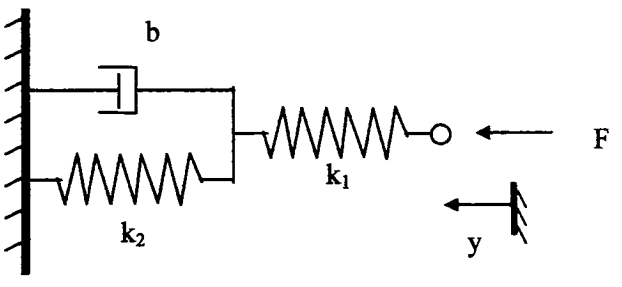

Figure 6 Three-parameter model of a viscoelastic material

The free end of the model is subjected to a harmonic force (F). Assuming a harmonic response leads to a relationship between the force and the displacement (y) of the free end as shown in equation 3.

$$F = \left[\frac{-k_1(k_2 + ib\omega)}{k_1 + k_2 + ib\omega} \right] y \qquad (3)$$

The mechanical impedance (Z) is enclosed in brackets and represents both the stiffness and damping characteristics of the material. The mechanical impedance of a linear spring is purely real and that of a viscous damper (dashpot) is purely imaginary. It is customary to represent the mechanical impedance in terms of the real part called the modulus (E), and the ratio of the imaginary part to the real part called the loss factor (δ) as shown in equation 4.

$$Z = E(1 + i\delta) \qquad (4)$$

The modulus and loss factor of a generic three parameter model are plotted as functions of frequency in figures 7 and 8 respectively. Note that the loss factor reaches its maximum value while the modulus is in transition from a soft rubbery state to a much stiffer glassy state[7].

More sophisticated models of viscoelastic materials account for non-linearity and temperature dependence of the material properties. The appropriate viscoelastic damping material must be selected for the anticipated operating temperature and frequency conditions. Damping effectiveness drops considerably as the temperature or frequency deviates from the design range.

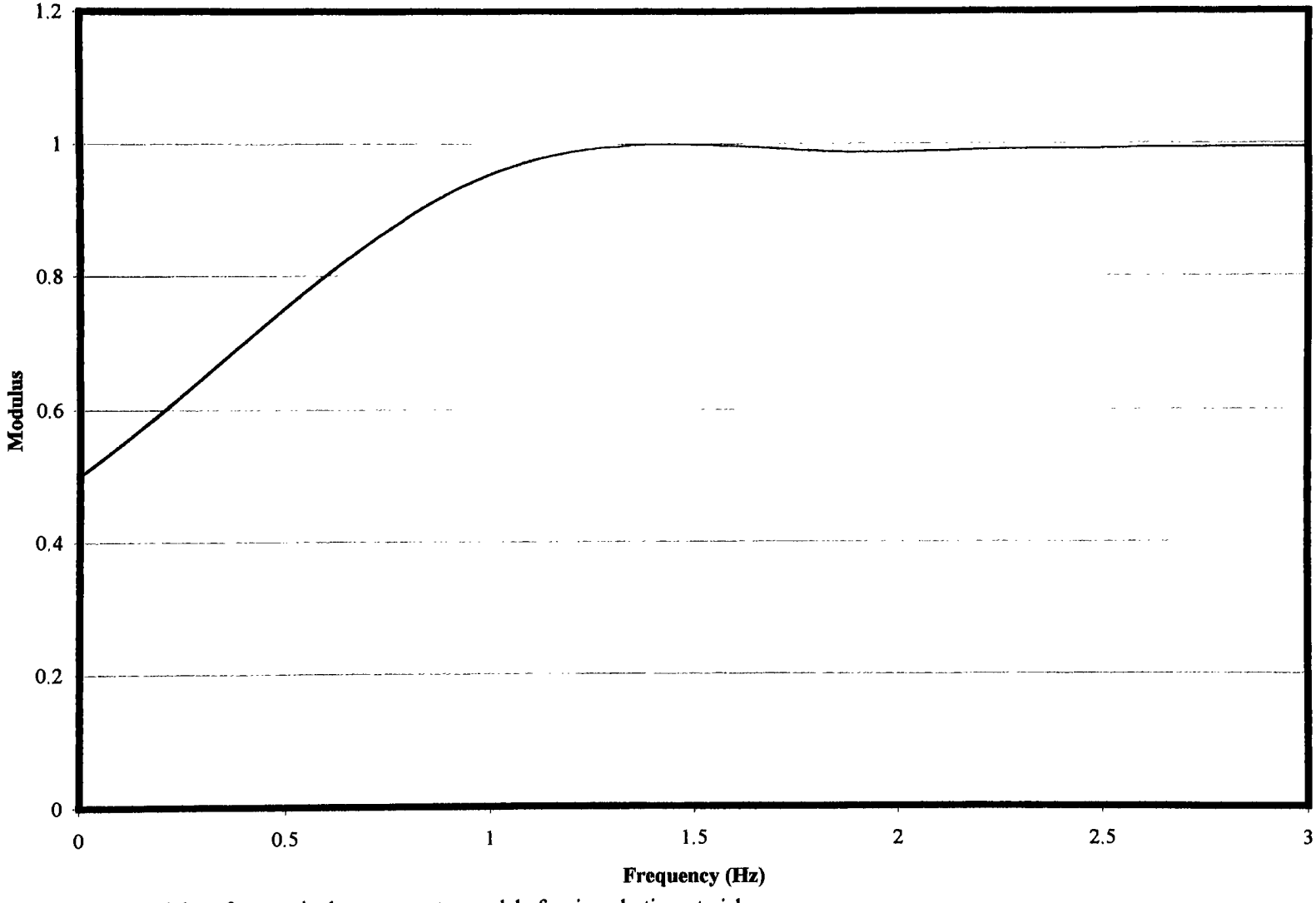

Figure 7 Modulus of a generic three parameter model of a viscoelastic material

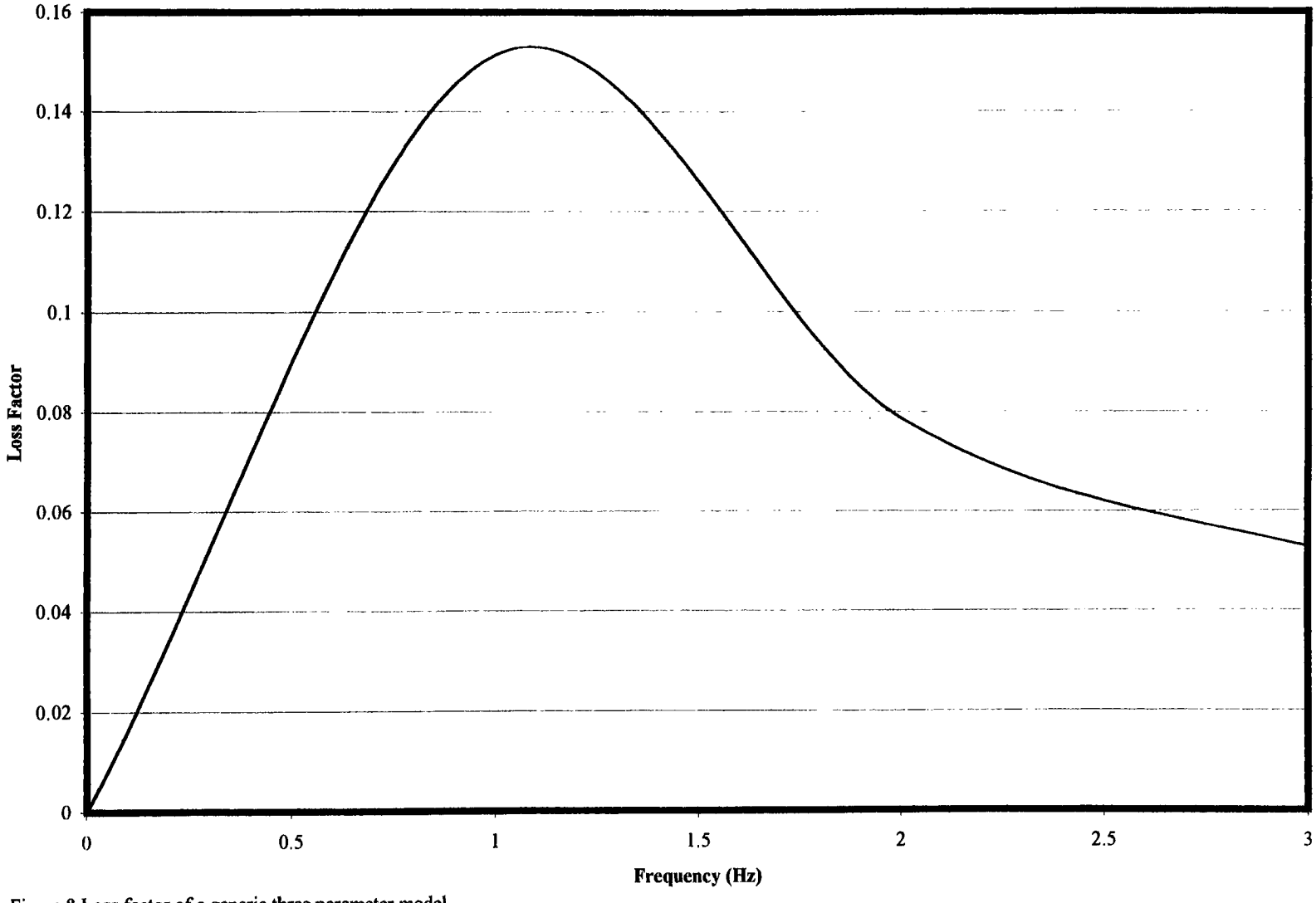

Figure 8 Loss factor of a generic three parameter model

Piezoelectric Materials

Piezoelectric materials have also proven useful for vibration control. Pierre Curie discovered the piezoelectric effect in 1880 when he demonstrated that an electric potential (voltage) develops in some crystals, such as quartz, when they are stressed. A year later Curie also demonstrated the converse effect: The crystals deform (strain) when an electric voltage is applied to them. This property of bi-directional energy transformation makes it possible to couple electrical and mechanical systems with piezoelectric materials.

The modern piezoelectric ceramics including lead ziconate titanate (PZT) became available after World War II. As early as 1956, the suitability of piezoelectric materials to structural vibration control was recognized by Olsen[12]. Piezoelectric elements are particularly appropriate for suppressing vibration of light beam-like or plate-like structures because piezoelectric elements are limited to small strains.

Electrically, a piezoelectric element can be modeled as a capacitor and current source in parallel as shown in figure 9. This model is accurate so long as the frequency of operation is below the resonant frequency of the piezoelectric element. The natural frequency of piezoelectric elements is typically on the order or 10^4 Hz[13]. The charge produced by the current source is proportional to the applied mechanical stress. The electromechanical coupling properties of piezoelectric elements have only a mild temperature and frequency dependence.

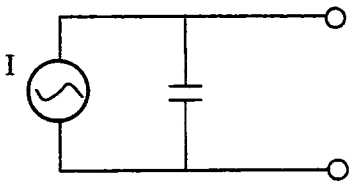

Figure 9 Schematic diagram of a piezoelectric element

Experimental Work

The cost and weight of vibration control treatments can be reduced by only applying the treatments to part of the structure. An understanding of mode shapes of the frequencies of concern is necessary to determine the best location for a damping treatment. For example, the energy dissipated per cycle by a viscous damping treatment is proportional to the damping coefficient and the square of the strain. A treatment with a given damping coefficient will therefore be most effective where the strain energy is greatest. For beam and plate-like structures, the strain energy is greatest where the radius of curvature is minimized. In other words, it would be undesirable to place a damping treatment in the vicinity of a node because strain is required for energy dissipation.

To achieve maximal damping for a structure as a whole, the damping provided by a treatment that partially covers the structure must be optimized. For partial damping treatments, the damping alters the mode shape and produces a non-linear relationship between the damping coefficient and the amount of energy dissipated. For small damping coefficients, the amount of energy dissipated increases with the amount of damping because the mode shape is virtually unchanged. However, for large damping coefficients, the amount of energy dissipated decreases as the damping rises because treatment rigidifies the structure in its vicinity. At some intermediate level of damping, the energy dissipated by the damping treatment is optimized.

To be consistent with Dr. Ghoneim's model, the EMSD treatment was evaluated on a cantilever beam that was excited by base motion. An aluminum beam with dimensions of 0.318x1.27x25.4 cm was used. A pair of EMSD elements covering 10% of the length of the beam was applied symmetrically to the beam as shown in figure 10. The EMSD was located at the root of the beam where the strain energy is greatest and consequently the treatment would be most effective.

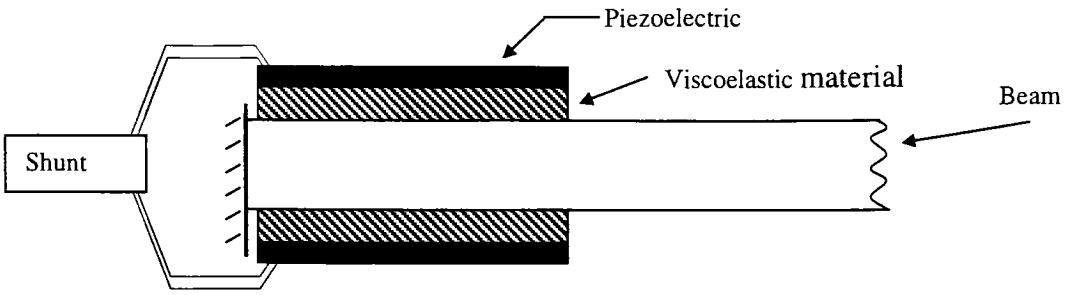

Figure 10 Diagram of a beam treated with the EMSD

Lead ziconate titanate (PZT) piezoelectric elements from Sensor Technology (BM-532) were used in the EMSD treatment. The dimensions of the piezoelectric elements were 2.54x1.27x0.102 cm. The manufacturer's specifications indicate that each element has a capacitance of 7.1 nF[13]

The treatments were assembled and bonded to the beam with an epoxy adhesive. A variety of epoxy and cyanoacrylate adhesives was tested. The adhesives were tested by bonding a 0.24x2.54x1.27cm piece of aluminum to a beam and looking for abnormalities or changes in the frequency response functions. The results for all of the adhesives were comparable. The cyanoacrylates were dismissed because they are known to be very weak in shear. An epoxy adhesive with a low viscosity was selected to allow the application of a thin layer of adhesive.

Two beams were treated with the EMSD. Both beams were treated with the same type of piezoelectric elements, but one beam was treated with a room temperature viscoelastic material (DYAD606), and the other was treated with a high temperature material (DYAD609). The manufacturer of the viscoelastic materials, Soundcoat, recommends DYAD606 for temperatures between 10 and 66°C, and DYAD 609 for temperatures between 49 and 140°C. Both types of viscoelastic material had a thickness of 0.051cm. Graphs of the moduli and loss factors of these two viscoelastic materials may be found in Appendix B.

The fixed end of the beam was attached to a linear bearing to limit motion to the direction transverse to the beam as shown in figure 11. A precision ball slide from Techno-Isel (part number H11D81-S3015) was used. The ball slide was secured to a heavy steel plate (with dimensions of 1.9 x 12.5 x 41 cm).

A shaker was used to excite the beam as shown in figure 11 with base motion. The shaker was a B&K 4809 with a 10lb rating. A stinger made of threaded steel rod (#10-32) connected the beam mount to the shaker. Foam was used to support the shaker in a cradle made from a piece of channel iron. The cradle was not connected to the steel plate on which the linear bearing was mounted.

The shaker was driven with a bin-centered random multi-sine signal from a computer based spectrum analyzer. The acceleration of the beam mount was measured with a PCB U352B65 accelerometer. The maximum amplitude of excitation was 250cm/s^2. Another accelerometer of the same type was placed at the free end of the beam, and the frequency response function (FRF) was measured for each beam.

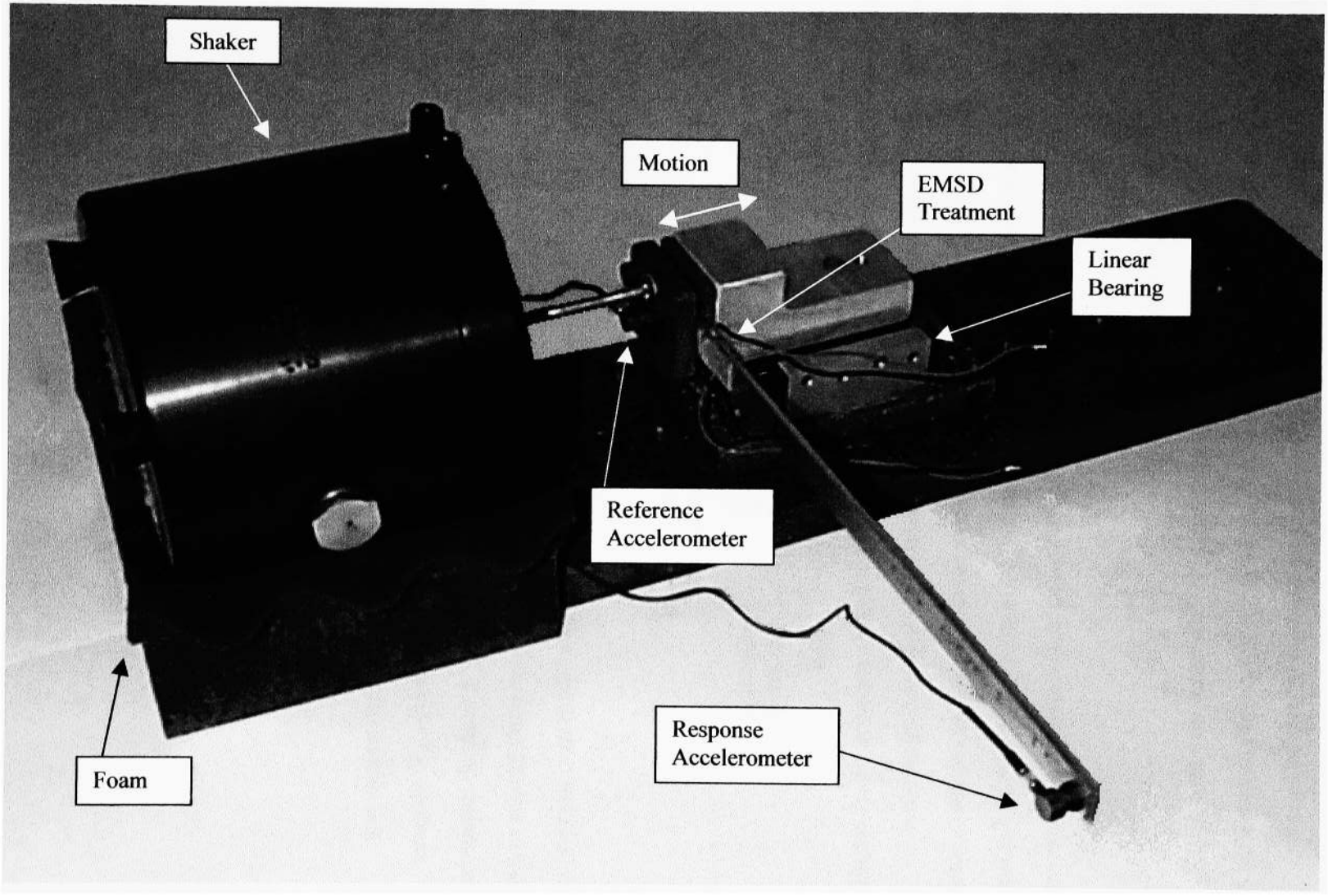

Figure 11 Experimental apparatus

Two synthetic inductors were constructed. One inductor was tuned to the second natural frequency of the treated beam (235 Hz) and the other inductor was tuned to the third natural frequency (650 Hz). FET op-amps (LF-412) and polypropylene capacitors were used in the synthetic inductors to minimize their internal resistance.

A diagram of the shunt circuit is shown in figure 12. The piezoelectric elements are connected in parallel rather than in series because a low input voltage to the shunt is desirable. The synthetic inductor will not behave as an inductor if the input voltage exceeds the supply voltage to the op-amps. The polarity of the piezoelectric elements is reversed because flexure of the beam simultaneously produces compressive stress in one element and tensile stress the other element.

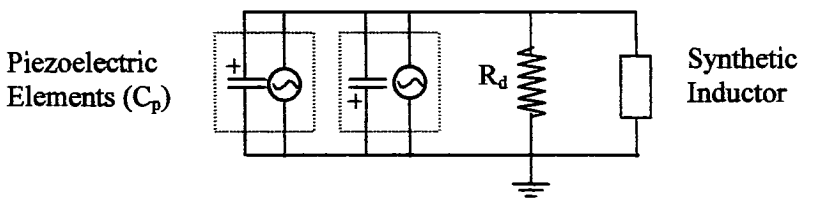

Figure 12 Piezoelectric elements and shunt

The component values and approximate resonant frequency (based on equations 1 and 2) of the shunted piezoelectric elements are given in table 1. Note that the combined capacitance of the piezoelectric elements in parallel is twice that of an individual element. A damping resistance was connected in parallel with the inductor. The resistance was adjusted to achieve the optimum damping. Note that throughout this experiment, the criteria for damping optimization is a horizontal line between points S and T in figure 5.

Table 1

R_1 (Ω)	R_2 (Ω)	R_3 (Ω)	R_4 (Ω)	C (F)	C_p (F)	Frequency (Hz)
1.79E+04	2.18E+03	2.75E+03	4.70E+04	3.30E-08	1.42E-08	225.94
9.93E+03	2.20E+03	2.71E+03	1.19E+04	3.30E-08	1.42E-08	609.39

Before collecting data, the linearity of the system was verified as shown in Appendix D by measuring the peak response as a function of the amplitude of excitation. Data was collected under three temperature conditions: A low temperature test was conducted at -8°C by placing the apparatus in a freezer. A room temperature test was conducted at 25°C in the vibration laboratory. A high temperature test was conducted at 55°C using an environmental control chamber in the Packaging Science Department. Modal damping ratios for the second and third modes were extracted from the FRFs by curve fitting with STAR Modal.

Results and Discussion

Frequency response functions for each beam were measured from 1 to 1000 Hz at three temperatures (-8°C, 25°C, and 55°C). The untreated beam was tested as a baseline. The treated beams were tested without a shunt to determine the damping achieved by the conventional constrained layer damping. Finally, the piezoelectric elements were shunted with an inductor (tuned to either the second or third mode) and the optimized damping resistance. Samples of the results are shown in figures 13 through 16.

Figures 13 and 14 show the second mode of the beam treated with DYAD 609 at 55°C and 25°C respectively. The conventional constrained layer treatment provides nearly optimal damping at 55°C and reduces the peak by 24dB. The EMSD reduces the peak only slightly further for a total reduction of 26dB. At 25°C, the conventional treatment only reduced the peak by 14dB and the EMSD provides the additional damping required for a total peak reduction of 29dB.

Figures 15 and 16 show the second and third modes respectively of the beam treated with DYAD 606 at a temperature of 25°C. The conventional constrained layer treatment reduces the peak amplitude of the second mode by 23 dB. The EMSD reduces the peak 8 dB further for a total reduction of 31dB. The conventional constrained layer treatment is less effective on the third mode where it reduced the peak by 10dB. The supplemental damping from the EMSD reduces the peak 8 dB further for a total reduction of 18dB.

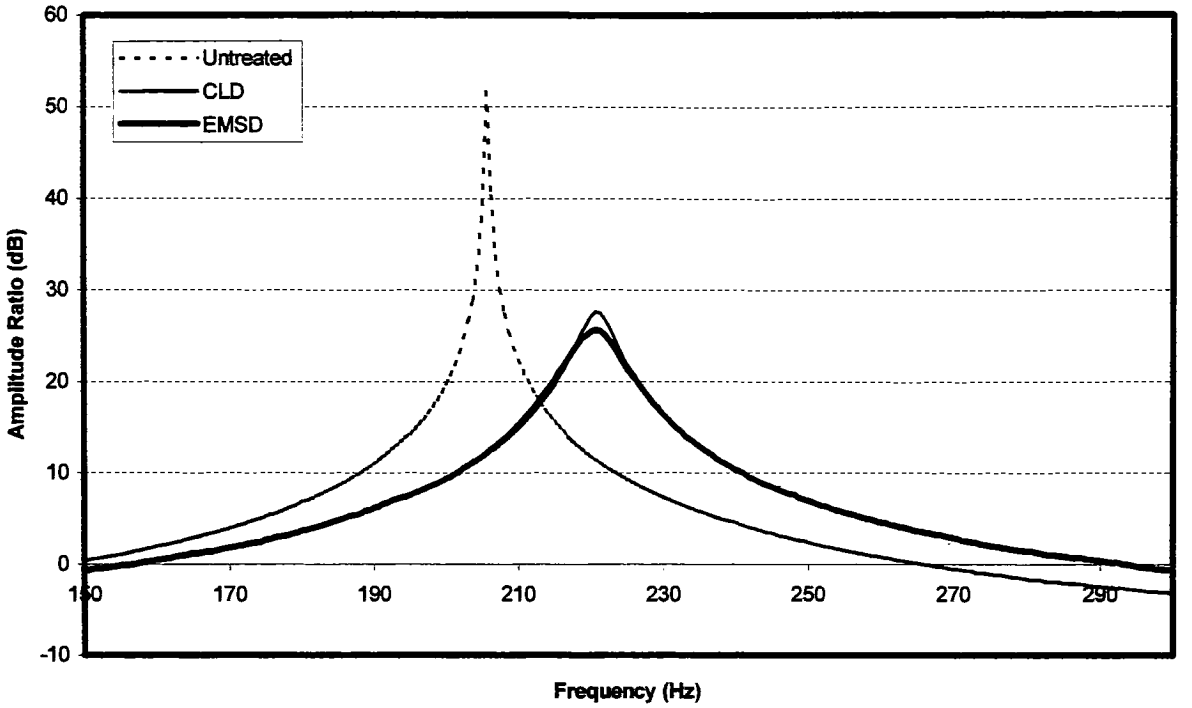

Figure 13 Frequency response function in the vicinity of the second natural frequency of the beam treated with DYAD 609 at a temperature of 55C

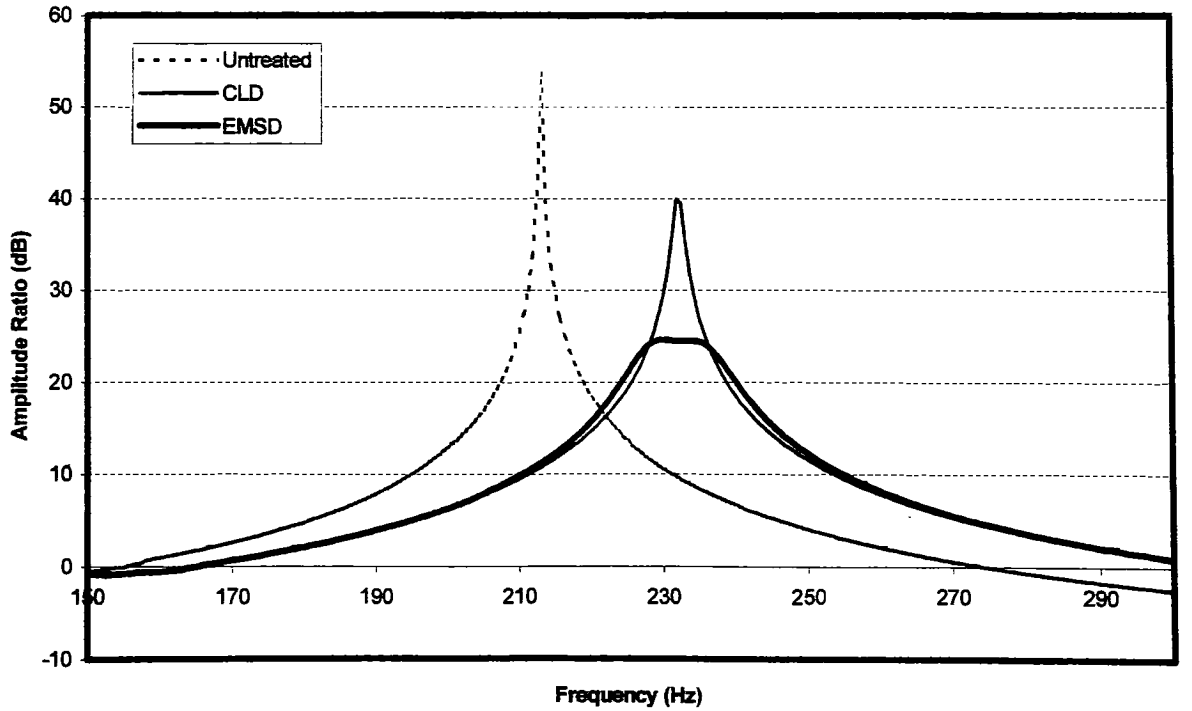

Figure 14 Frequency response function in the vicinity of the second natural frequency of the beam treated with DYAD 609 at 25C

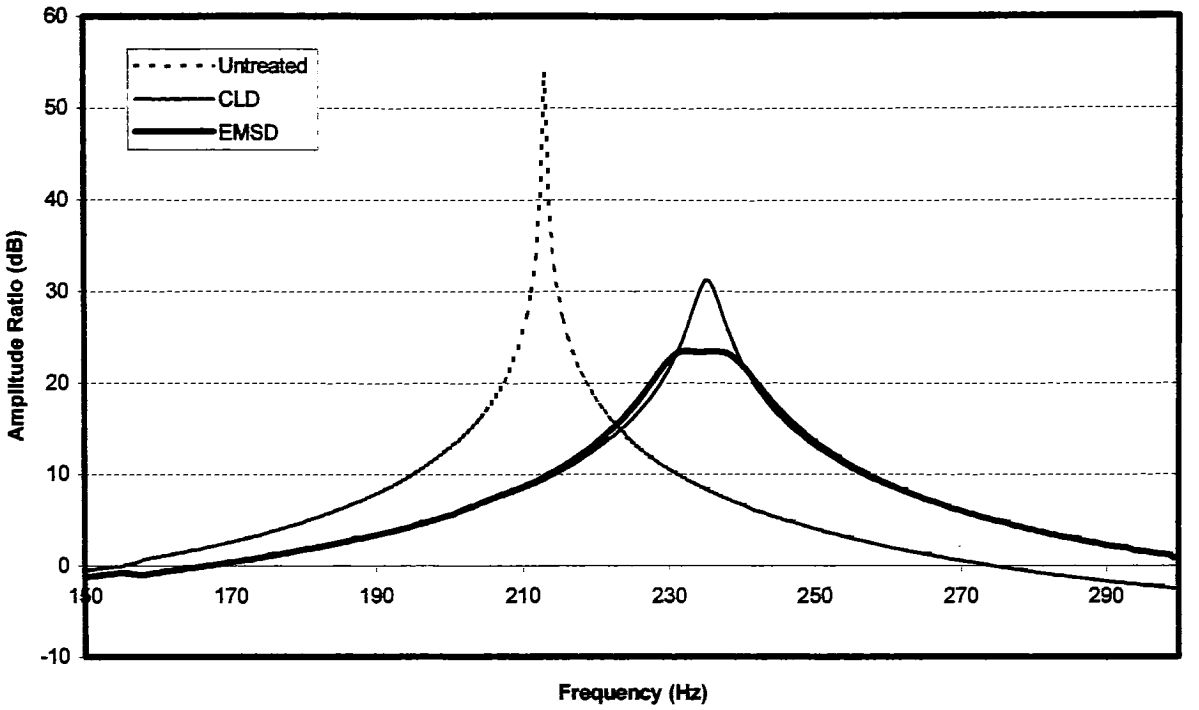

Figure 15 Frequency response function in the vicinity of the second natural frequency of the beam treated with DYAD 606 at a temperature of 25C

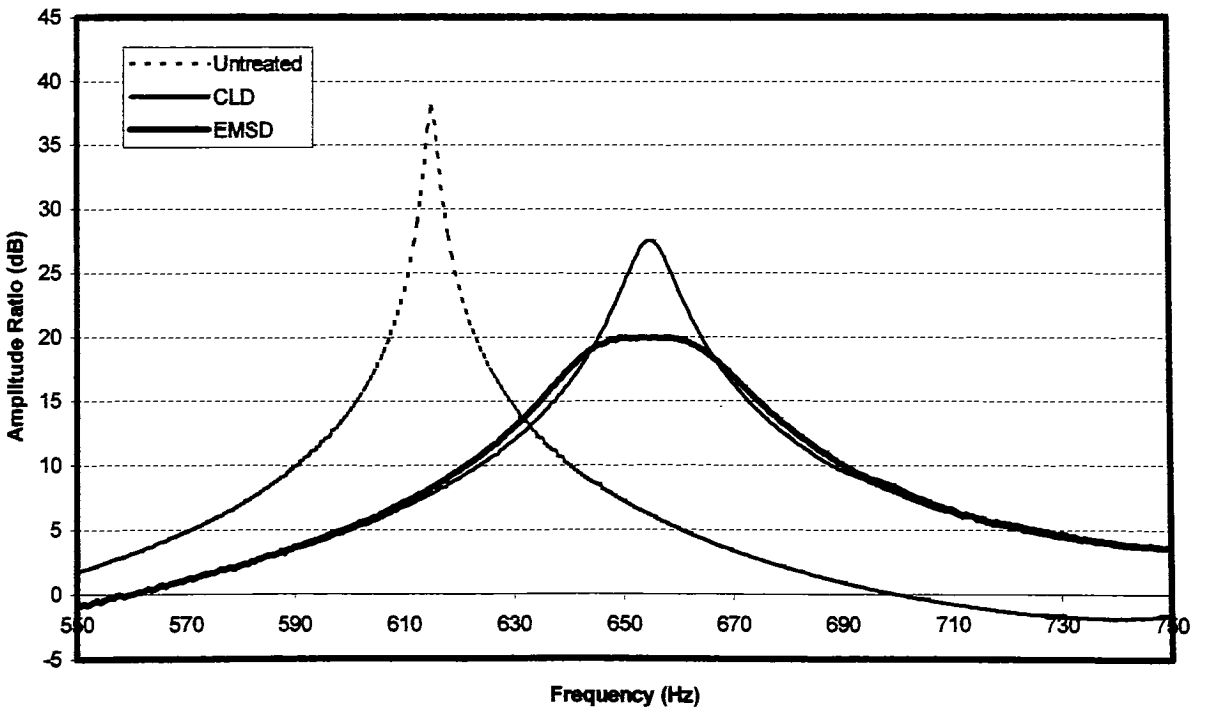

Figure 16 Frequency response function in the vicinity of the third natural frequency of the beam treated with DYAD 606 at a temperature of 25C

The peak amplitudes of the second and third modes are plotted as functions of temperature for the beam treated with DYAD 609 in figures 17 and 18. According to the graphs in Appendix B, the loss factor of the viscoelastic material is greatest at approximately 85°C for mode 2, and at approximately 110°C for mode 3. As expected, figures 17 and 18 show that the constrained layer is most effective at 55°C for both modes. The EMSD can only improve the peak reduction by a few decibels (dB) because the damping provided by the constrained layer is nearly optimal. At the lower temperatures, the viscoelastic material is less effective and the EMSD significantly enhances the performance of the constrained layer.

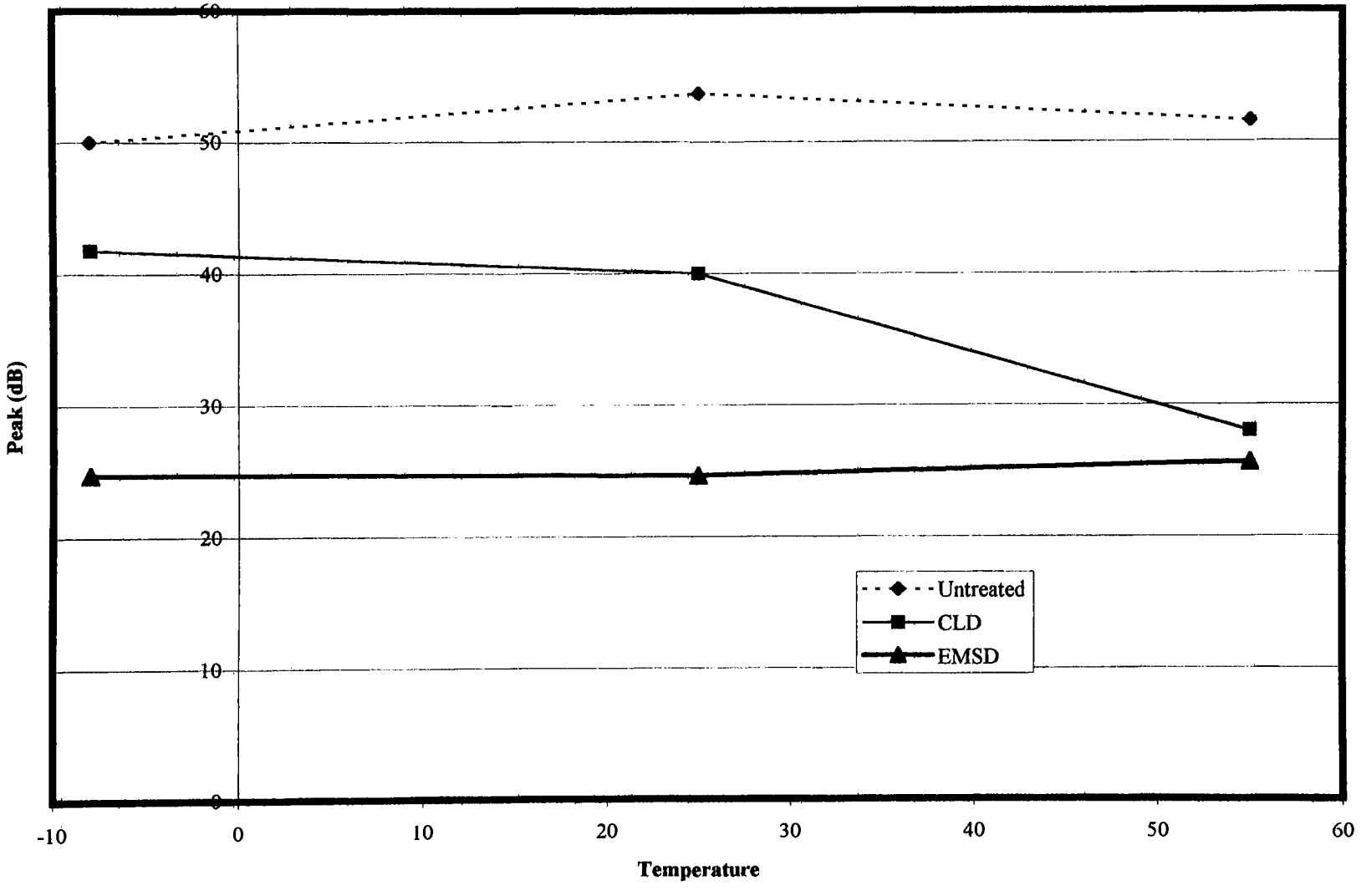

Figure 17 DYAD 609 mode 2 temperature summary

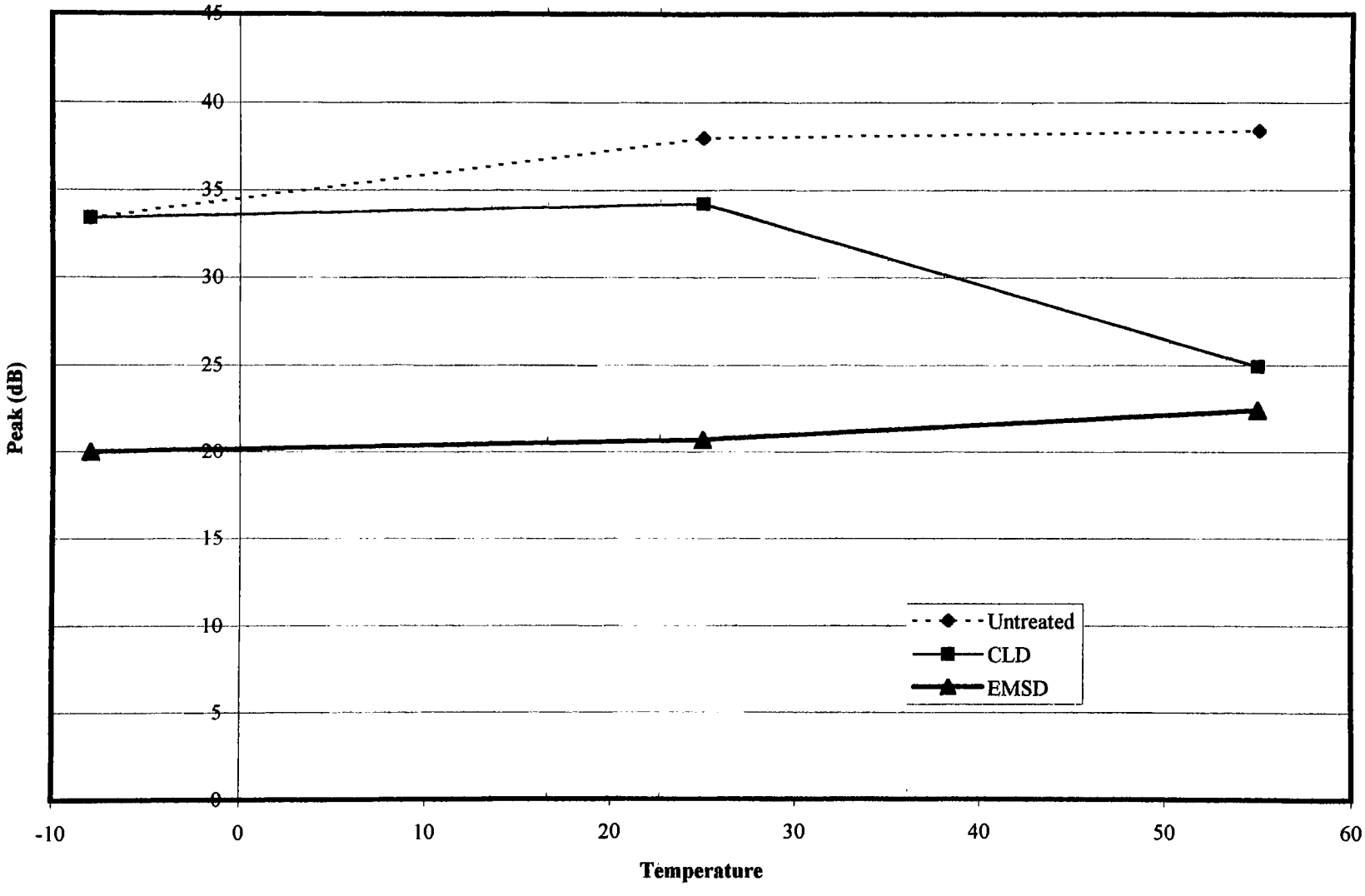

Figure 18 DYAD 609 mode 3 temperature summary

In figures 19 and 20 the peak amplitude is plotted as a function of temperature for the beam treated with DYAD 606. According to graphs in Appendix B, the loss factor of the viscoelastic material is greatest at approximately 45°C for mode 2, and at approximately 55°C for mode 3. However, the constrained layer is not very effective at 55°C. This may be attributable to the fact that the damping depends on the thickness of the viscoelastic material as well as on the loss factor. It is also noted that the EMSD can no longer increase the amount of damping provided by the constrained layer because the viscoelastic material is too soft to transmit energy to the piezoelectric elements. The graphs in Appendix B indicate that the shear modulus is an order of magnitude lower than at 25°C. Greater peak reductions are achieved at 25°C where the constrained layer provides less than the optimum damping. At the lower temperatures, the EMSD supplements the damping from the constrained layer to achieve the optimum damping for the system.

The peak amplitudes of the second and third modes of the beams treated with DYAD 606 and 609 are compared in figure 21. According to graphs in Appendix B, the loss factor of both viscoelastic materials is greater for mode 2 than mode 3 at all cases except DYAD 606 at 55°C. The constrained layer is more effective on the second mode than the third in all cases except when the damping exceeded optimum value (DYAD 606 at 55°C) because the viscoelastic materials become less effective at higher frequencies. EMSD extends the effectiveness of the constrained layer treatment over a broader range of frequencies so long as the optimal damping is not exceeded.

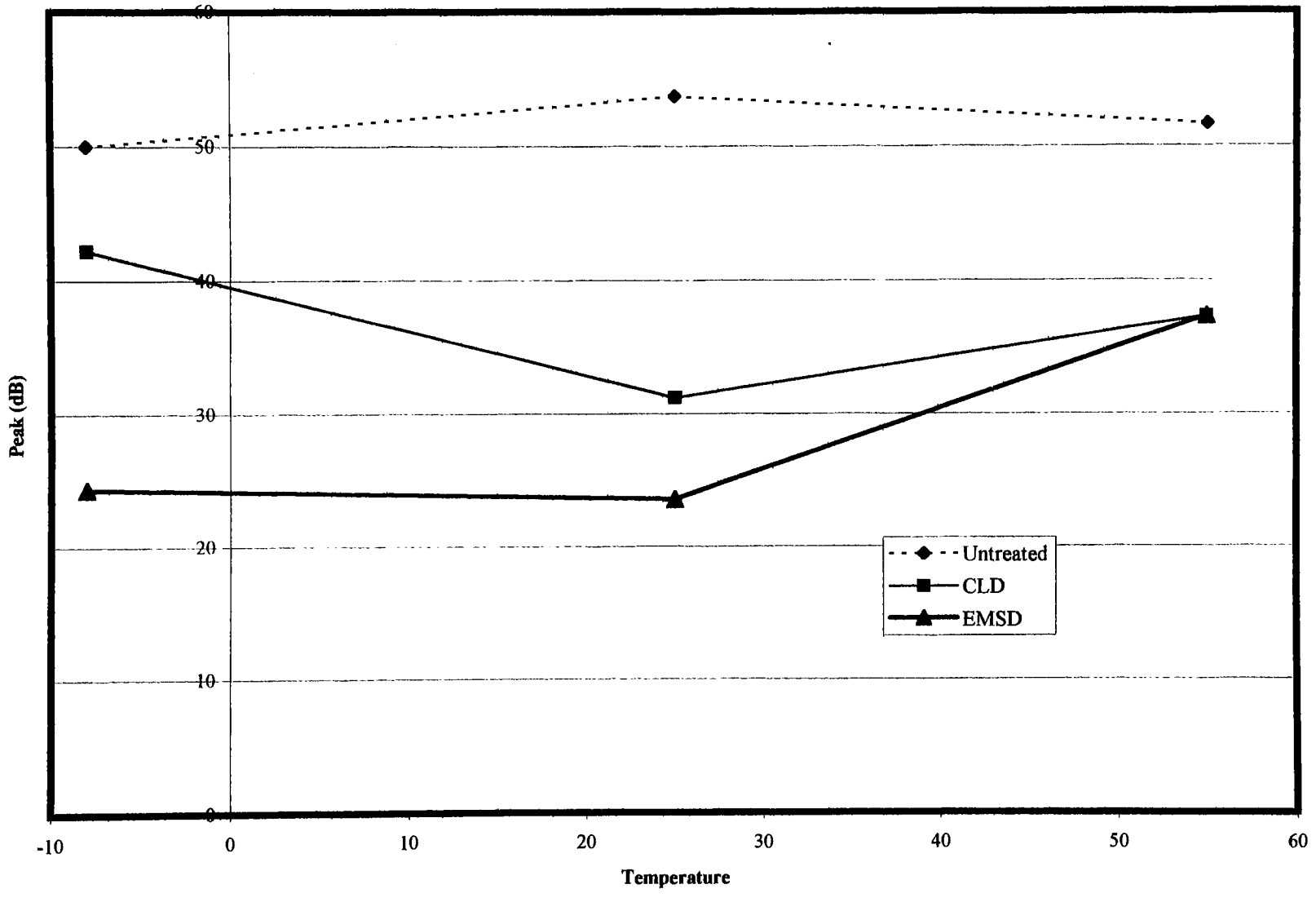

Figure 19 DYAD 606 mode 2 temperature summary

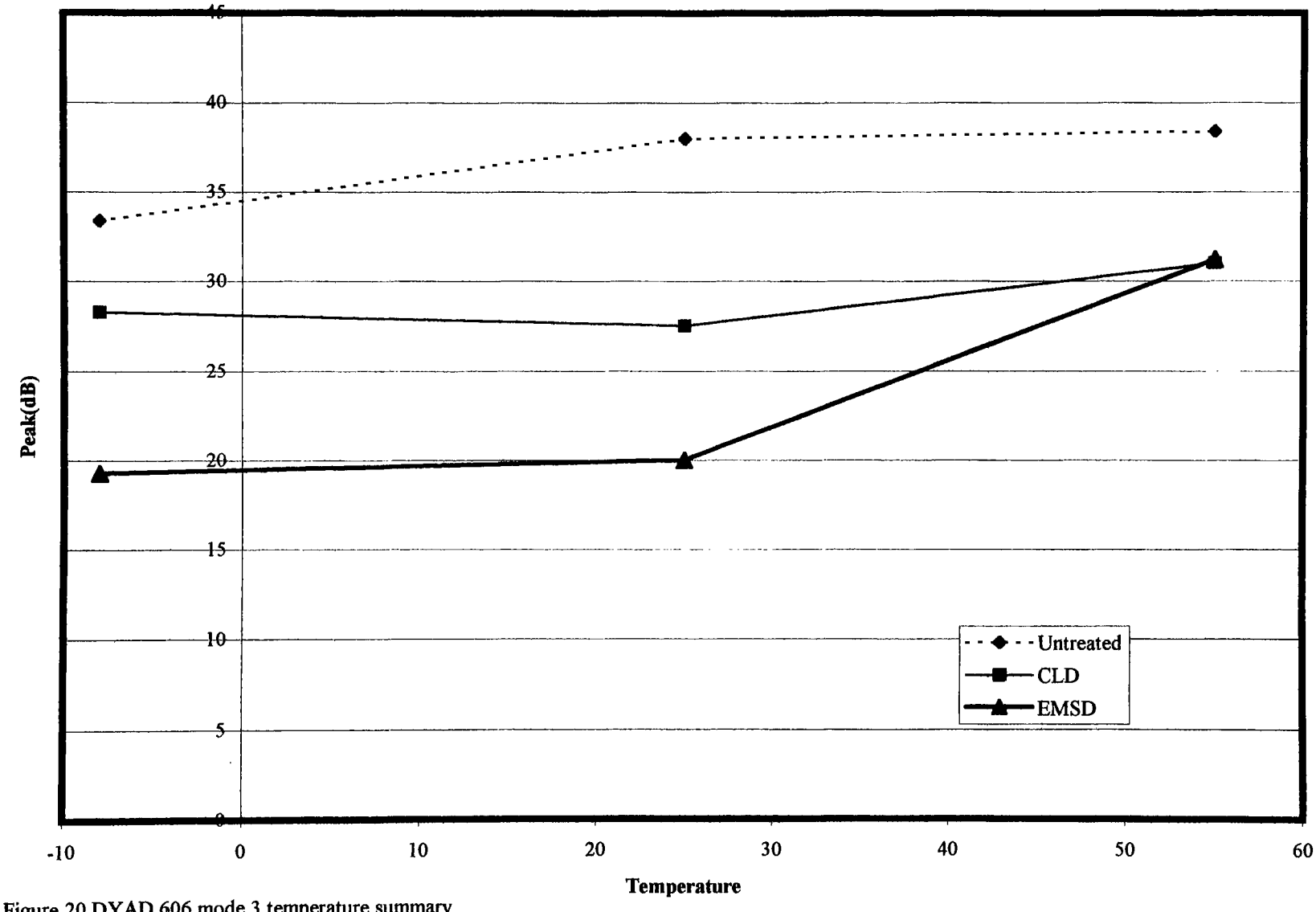

Figure 20 DYAD 606 mode 3 temperature summary

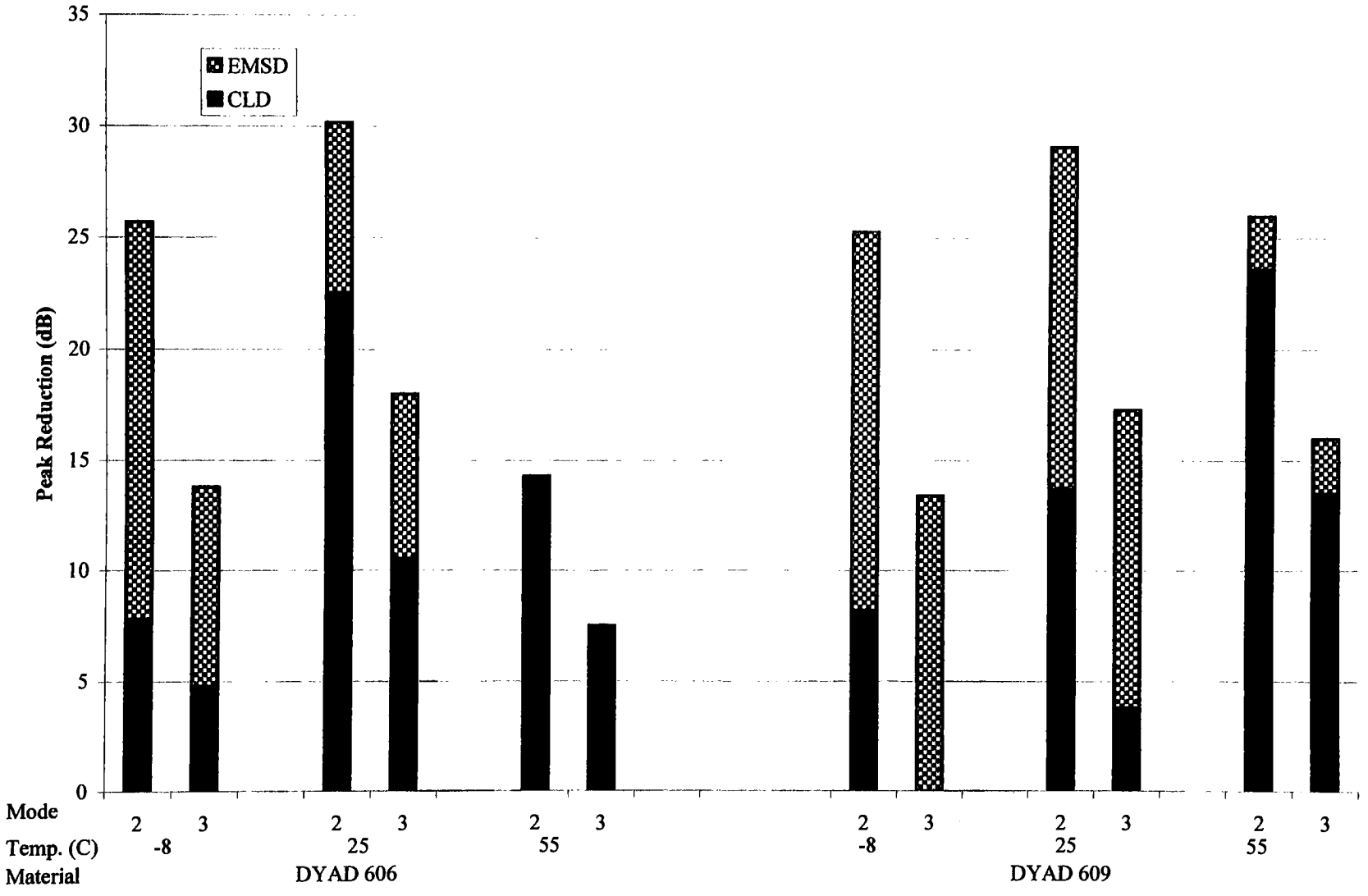

Figure 21 Effectiveness of the constrained layer and EMSD as functions of frequency

The experimental results were compared with those obtained from Dr. Ghoneim's finite element model. Figure 22 shows the analytical frequency response functions for the beam treated with DYAD 606 in the vicinity of the second mode and at a temperature of 25°C. Comparison of these analytical results with the corresponding experimental results in figure 15 indicates that, in general, the model is stiffer. The excess stiffness of the model may be attributed to the use of generic material parameters, modeling the accelerometer as a point mass, and the assumption of a perfectly cantilevered beam (see Appendix C). Furthermore, the analytical results indicate that the EMSD treatment suppresses the peak vibration amplitude more than was observed experimentally. The difference may be attributed to the assumption of pure electronic components (inductance, capacitance, and resistance) in the analysis. However, in general the agreement between the analytical and experimental results is good.

The damping ratios (ζ) for the second and third modes of vibration were extracted with STAR Modal. Table 2 presents the damping ratios for the untreated beam, the beams treated with conventional constrained layer treatments, and the beams treated with the EMSD. The table also includes the inductance and damping resistance of the shunts. The EMSD treatment consistently introduces more damping to the system than conventional constrained layer treatment, thereby providing more vibration suppression in the vicinity of the natural frequencies.

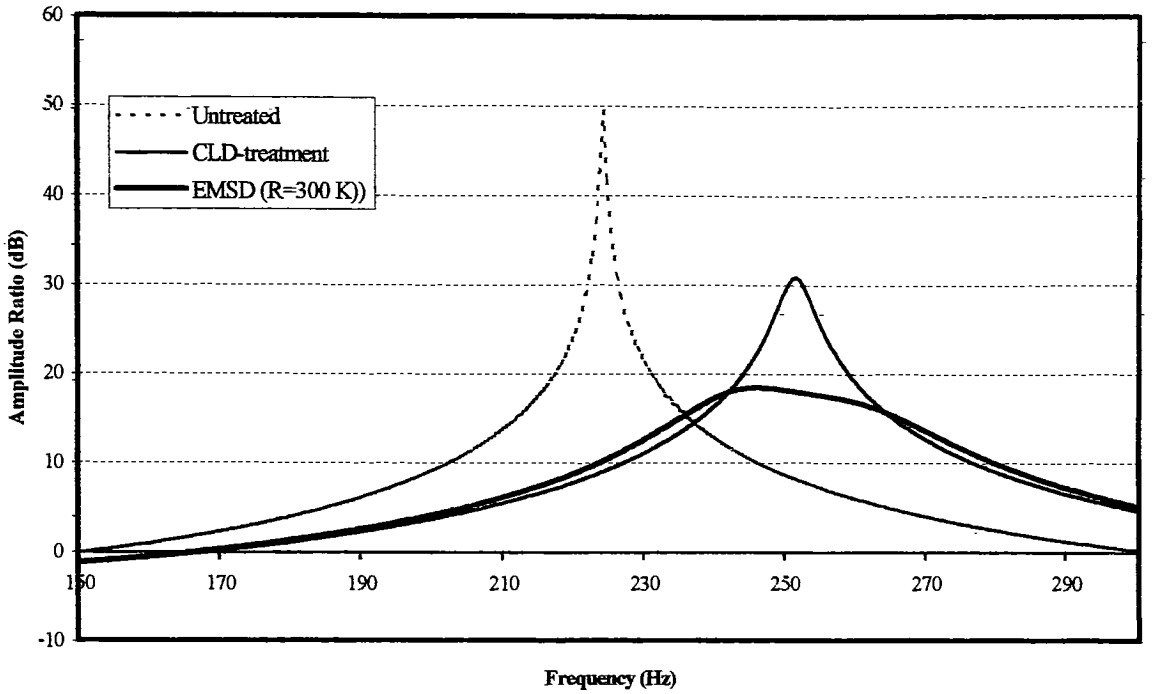

Figure 22 Dr. Ghoneim's FEM results (DYAD 606 at 25C)

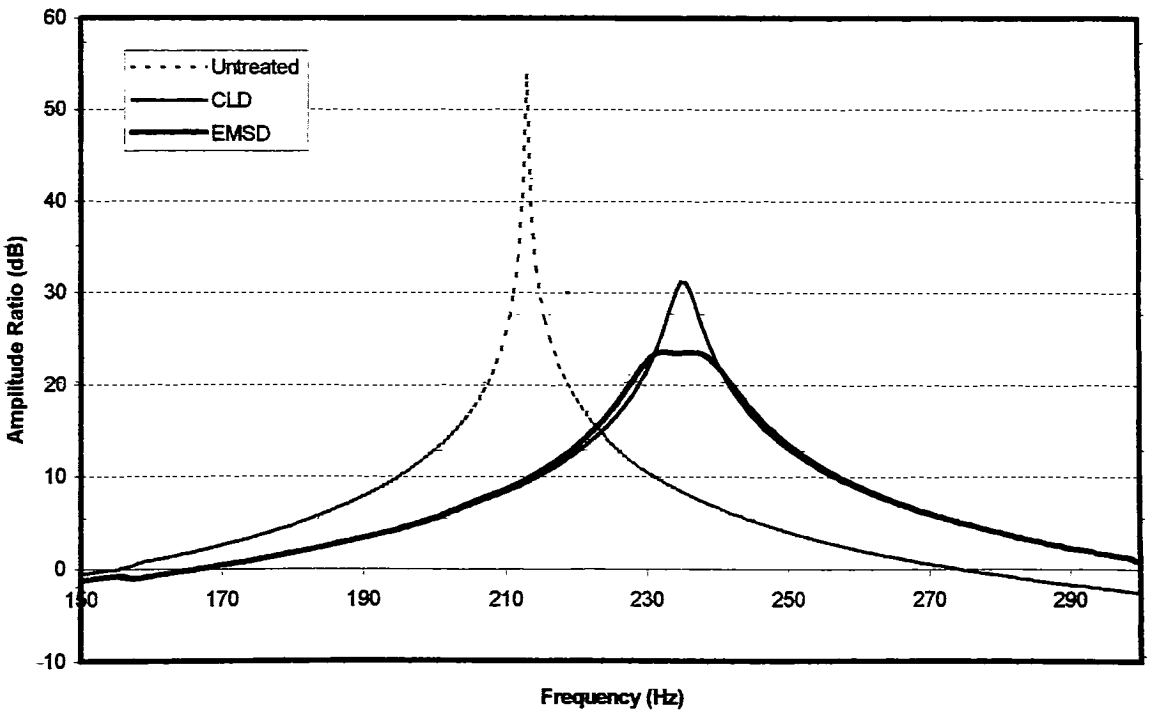

Figure 23 Experimental results (DYAD 606 at 25C)

Table 2 – Modal Damping Ratios

Mode	Temp (C)	Material (DYAD)	Inductor (H)	Resistor (kΩ)	$\zeta_{Untreated}$ (%)	ζ_{CLD} (%)	ζ_{EMSD} (%)
2	-8	606	35.7	1290	.05	.22	2.3
3	-8	606	4.8	640	.29	.76	2.8
2	-8	609	36.1	179	.05	.21	2.1
3	-8	609	4.8	776	.29	.35	2.4
2	25	606	28.7	2260	0.03	0.8	2.1
3	25	606	4.6	790	0.16	0.7	1.9
2	25	609	34.9	1790	0.03	0.3	2.0
3	25	609	4.8	775	0.16	0.3	2.0
2	55	609	33.2	∞*	.06	1.2	1.6
3	55	609	4.4	∞*	.13	0.8	1.2

* The internal resistance of the synthetic inductor did not allow optimization of the damping resistance.

Conclusion

Conventional constrained layer and active constrained layer damping are both effective vibration control methods for beam-like and plate-like structures. However, each method has disadvantages: Conventional constrained layer damping is only effective over a limited temperature and frequency range. Active constrained layer damping requires a complex controller. Electromechanical surface damping enhances the performance of conventional constrained layer damping without adding the complexity of active control. The EMSD technique enhances the damping effectiveness (peak amplitude suppression) at targeted resonant frequencies. Consequently, the EMSD may be used to extend the damping effectiveness of the constrained layer damping technique over a broader temperature and frequency range. The EMSD treatment increased the damping provided by the conventional constrained layer treatment so long as the viscoelastic material remained stiff enough to transmit strain energy to the piezoelectric element.

The damping provided by the EMSD treatment was changed by adjusting the damping resistor. This adjustment could be automated by replacing the damping resistor with a temperature dependant resistor (a thermistor). A multi-mode resonant shunt such as the one used by Hollkamp[14] could also be used to suppress more than one resonance peak simultaneously.

References

1 Singh, Sheikh, and Mitchell, "Viscoelastic Damping to Control Disk Brake Squeal", Sound and Vibration, October 1998, p.18

2 Bogue, Mulcahey, and Spangler, "Piezoceramic Applications for Product Vibration Control", Sound and Vibration, October 1998, p.24

3 Torvik, P.J. Ed., "The Analysis and Design of Constrained Layer Damping Treatments", Damping Applications for Vibration Control, p.85

4 SoundCoat, Inc., "Constrained Layer Damping Materials for Control of Noise and Vibration", Deer Park, New York

5 Baz, A., and Ro, J., "The Concept and Performance of Active Constrained Layer Damping Treatments", Sound and Vibration, p.18, March 1994

6 Shen, I.Y., "Hybrid Damping Through Intelligent Constrained Layer Treatments", Journal of Vibration and Acoustics, Vol 116, pp 341-349, 1994

7 Hagwood, N.W. and von Flotow, A, "Damping of Structural Vibrations with Piezoelectric Materials and Passive Electrical Networks", Journal of Sound and Vibration, 1991, vol 146 pp 243-268

8 Edberg, Bicos, Fuller Tracy, and Fechter, "Theoretical and Experimental Studies of a Truss Incorporating Active Members", J. of Intelligent Material Systems and Structures, Vol 3 pp 333-347, 1992

9 Wu, Shu-yau, "Piezoelectric Shunts with Parallel R-L Circuit for Structural Damping and Vibration Control", SPIE, Vol. 2720 pp.259-269, 1996

10 Ghoneim, "Electromechanical Surface Damping Using Constrained Layer and Shunted Piezoelectric", SPIE Proceeding: Smart Structures and Materials, Vol 1919-8, 1993

11 Ghoneim, "Application of the Electromechanical Surface Damping to the Vibration Control of a Cantilever Plate", Journal of Vibration and Acoustics, Vol 118, pp 551-557, 1996

12 Olson, H.F., "Electronic Control of Noise, Vibration, and Reverberation", Journal of the Acoustical Society of America, Vol 28, Number 5, 9/1956, p. 966

13 Sensor Technology Limited, Product Catalog, Collingwood, Ontario, Canada

14 Hollkamp, J., "Multimodal Passive Vibration Supression with Piezoelectric Materials and Resonant Shunts", Journal of Intelligent Material Systems and Structures", Vol 5, p. 49, 1994

15 Horowitz & Hill, The Art of Electronics, Cambridge University Press, New York, 1997

Appendix A

A synthetic inductor can be constructed with a capacitor, two operational amplifiers, and several resistors. When large inductance values are required, a synthetic inductor has several advantages over a conventional component. First, much larger inductance values can be achieved with synthetic inductors. Second, synthetic inductors weigh less than a traditional inductor. Third, the internal resistance of synthetic inductors tends to be less than that of conventional components. In other words, synthetic inductors have a higher "Q" value. Finally, inductance of synthetic inductors is easily adjustable.

The electrical impedance of a resistor (Z_r), capacitor (Z_c), and inductor (Z_l) are stated in equations 5, 6 and 7. In these equations, R is the resistance, C is the capacitance, L is the inductance, and ω is angular frequency.

$$Z_r = R \tag{5}$$

$$Z_c = \frac{1}{iC\omega} \tag{6}$$

$$Z_l = iL\omega \tag{7}$$

The synthetic inductor is based on a "negative impedance converter" (NIC)[15]. A negative impedance converter is shown in figure 24.

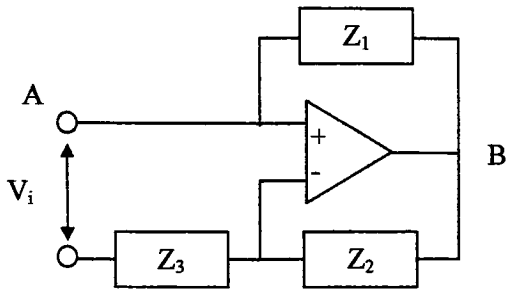

Figure 24 Negative impedance converter

When a voltage V_i is applied across the inputs of the NIC in figure 24, the operational amplifier (op-amp) increases the voltage at point B until both if its inputs are at the same voltage. Note that in practice the output of the op-amp can not exceed its supply voltage. Impedance's Z_2 and Z_3 form a voltage divider. The voltage at point B (V_b) is therefore given by equation 8.

$$V_B = \left(\frac{Z_2 + Z_3}{Z_3}\right)V_i \tag{8}$$

From Ohm's law, the current (I) through Z_a and through point A is given by equation 9.

$$I = \frac{V_i - V_B}{Z_1} \tag{9}$$

Substituting V_B from equation 8 yields the impedance of the negative impedance converter as stated in equation 10.

$$Z_{NIC} = \frac{-Z_1 Z_3}{Z_2} \tag{10}$$

The synthetic inductor is composed of two negative impedance converters. One negative impedance converter (NIC1) is nested within the second negative impedance converter as shown in figure 25. The impedance Z_4 of NIC2 is that of NIC1.

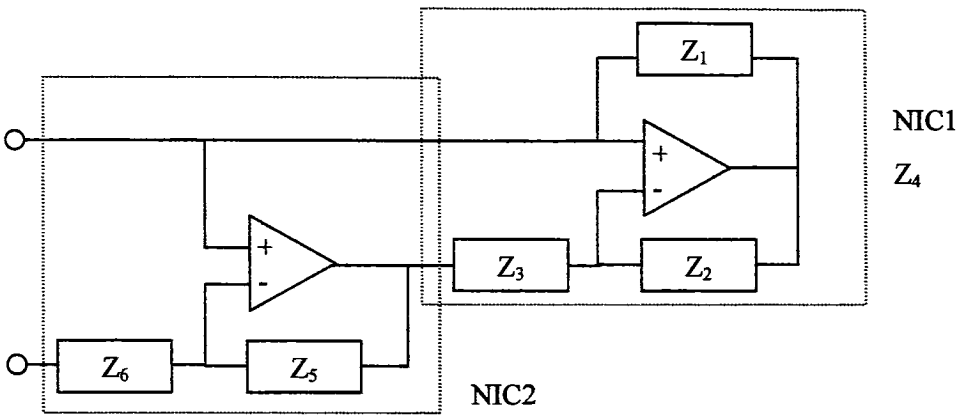

Figure 25 The synthetic inductor is composed of two negative impedance converters.

In the synthetic inductor, Z_5 is a capacitor and Z_1, Z_2, Z_3, and Z_6 are resistors. The impedance of the synthetic inductor is given in equation 11. Note that the impedance is imaginary and proportional to ω as stated in equation 7 for a pure inductor. The inductance (L) is the constant of proportionality contained within the brackets.

$$Z = i\left[\frac{R_1 R_3 R_4 C}{R_2}\right]\omega \qquad (11)$$

In practice, the impedance of a synthetic inductor is not purely inductive. Two of the most significant sources of impurity are the input impedance of the op-amp and the dissipation factor

of the capacitor. To minimize these effects, a FET op-amp and high quality (such as polypropylene) capacitor should be used.

To ensure proper performance of the synthetic inductor, care must also be taken to ensure that the output of the op-amps remains well below their supply voltages. Equation 8 can be used to calculate the output of the op-amps. An oscilloscope with a high input impedance (at least 1MΩ) must be used when measuring voltage produced by the piezoelectric elements because the oscilloscope can attenuate the signal.

Appendix B

The modulus and loss factors of Dyad 606 and 609 are plotted as functions of temperature and operating frequency in figures 26 and 27 respectively. These graphs were reproduced with permission from SoundCoat, Inc.

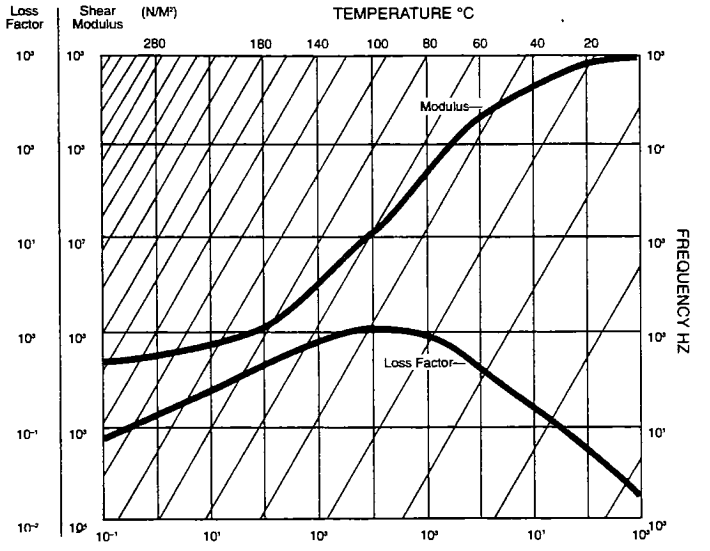

Figure 26 Modulus and loss factor of DYAD 606. © SoundCoat, Inc.

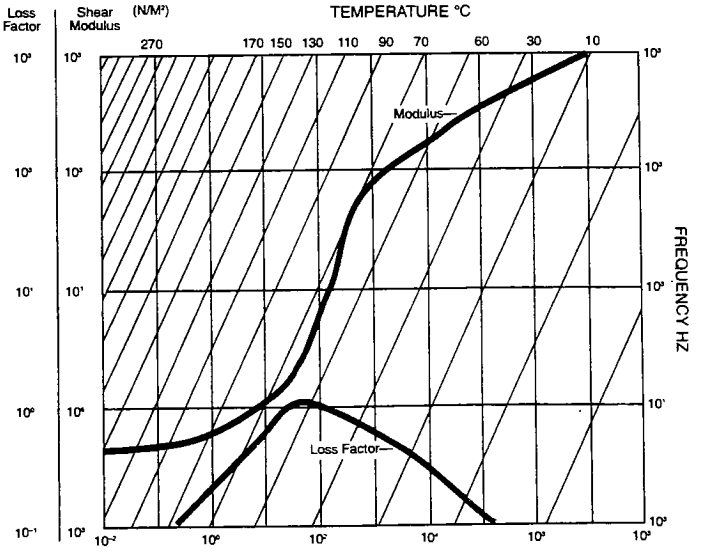

Figure 27 Modulus and loss factor of DYAD 609. © SoundCoat, Inc.

Appendix C

The elasticity of the linear bearing components allows small displacements in the 'constrained' degrees of freedom. These displacements can produce less than ideal boundary conditions for the cantilever beam. Of the six required boundary conditions at the root of the beam, translation in the 'Z' direction (see figure 28) and rotation about the 'Y' axis experience the greatest loads as the beam bends. Translation in the 'Z' direction is not effected by the elasticity of the bearing components because the slide is free to move in this direction. However, small angles of rotation about the 'Y' axis are possible due to the elasticity of the bearing components. Consequently, the bearing characteristics effect the boundary conditions of the beam.

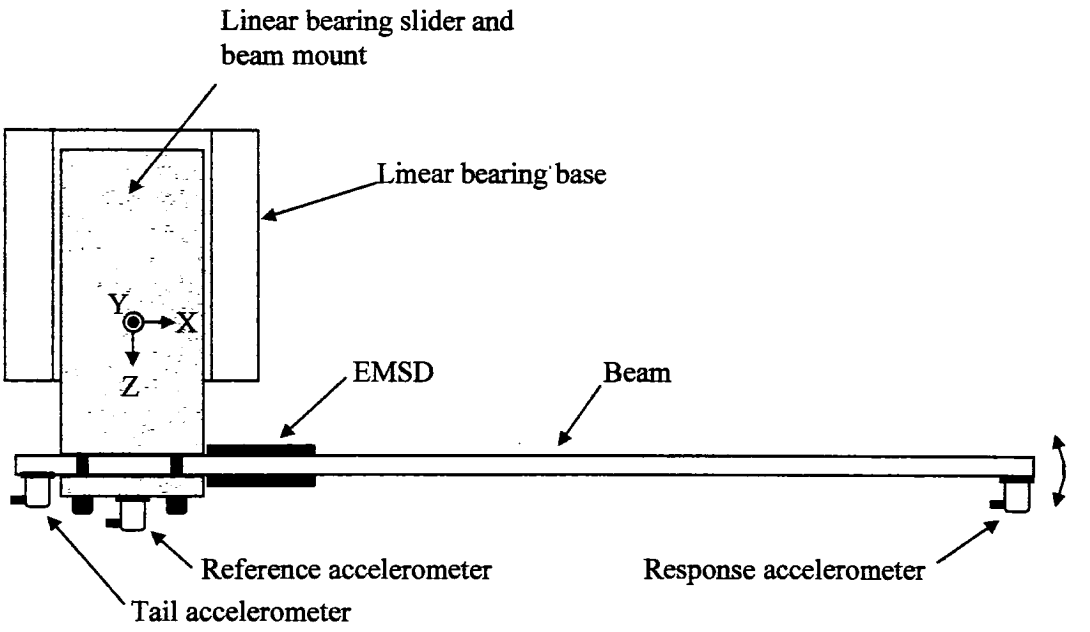

Figure 28 Diagram of the linear bearing and beam with accelerometers

The 'bearing effect' produced by torsion on the linear bearing can alter the frequency response function of the beam. The accelerometers used in this experiment can only sense linear motion in their axial direction (the 'Z' direction for both the reference and response accelerometers). The reference accelerometer will detect very little of the bearing effect acceleration because it is transverse to the accelerometers axis of sensitivity. However, the response accelerometer will detect some of the bearing effect acceleration and alter the frequency response function of the beam.

The angular acceleration that produces the bearing effect was measured by placing an accelerometer on the unused end (tail) of the beam. The tail was assumed rigid because it only extended about 1cm from the mount. The angular acceleration was determined by taking the ratio of the acceleration of the tail to that measured by the reference accelerometer.

The effect of the bearing on the FRF of the beam was minimized by adjusting the natural frequencies attributable to the bearing so that they did not coincide with the natural frequencies of the beam. The bearing effect frequencies were adjusted by changing the mass and moment of inertia of the bearing mount and by selecting a stiff singer. Figure 29 shows the frequency response function for the mount. The second and third natural frequencies of the beam produce the features at 213 and 615 Hz respectively. The first two bearing frequencies were tuned to 422 and 770 Hz respectively.

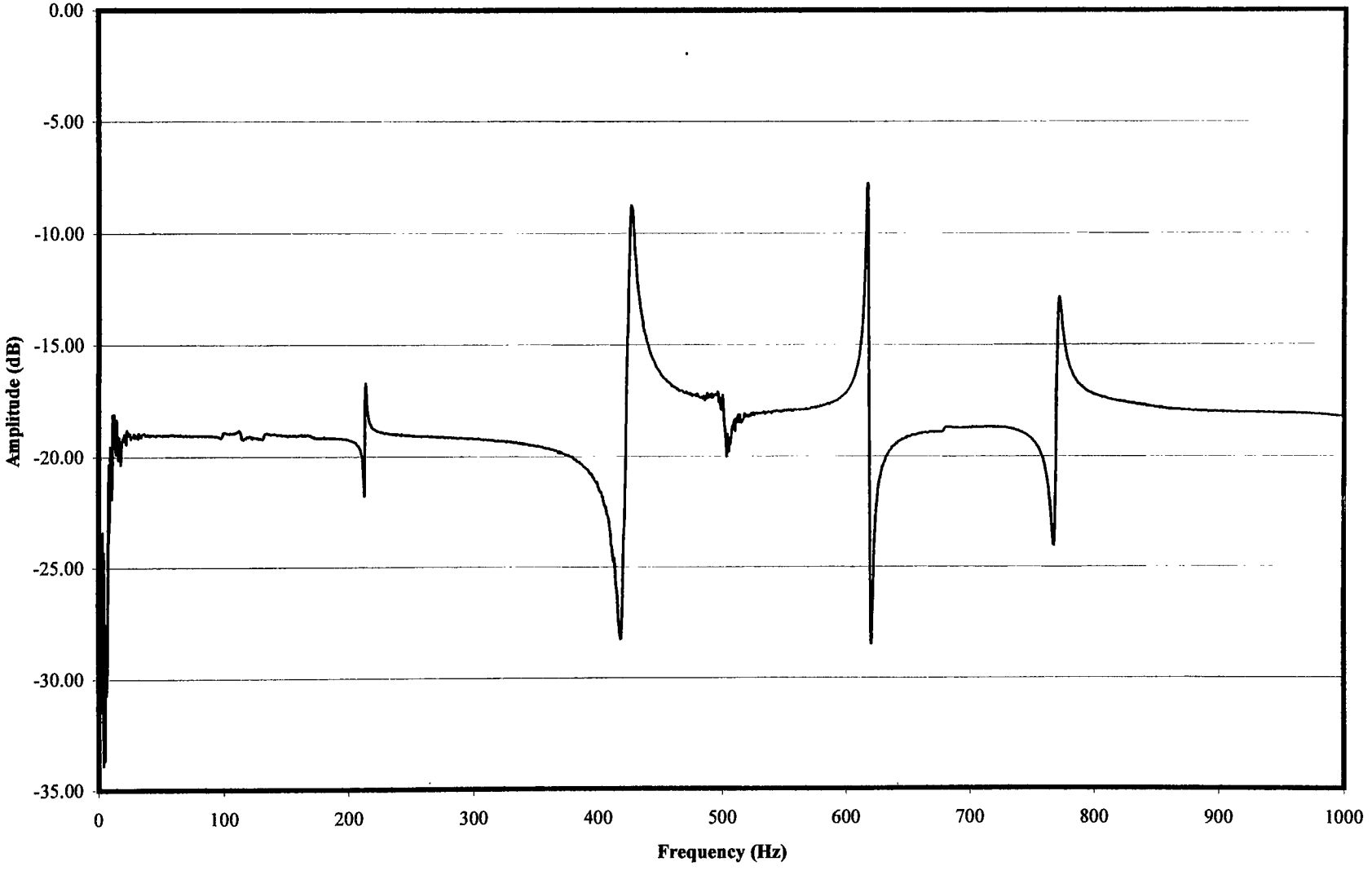

Figure 29 Frequency response function showing the bearing effect (Tail/reference)

Appendix D

The linearity of the system was verified by measuring the second and third natural frequencies of the beam as functions of the excitation amplitude. Linearity tests were conducted at room temperature on the untreated beam, and on both of the treated beams. Figures 30 through 33 show that the natural frequencies for excitation amplitudes between 25 and $8x10^3$ cm/s^2. The frequencies change less than 0.1% once the excitation amplitude falls below 850 cm/s^2. Two other problems also arose above 850 cm/s^2: The frequency response function became very noisy and the voltage across the inductor exceeded the supply voltage to the op-amps.

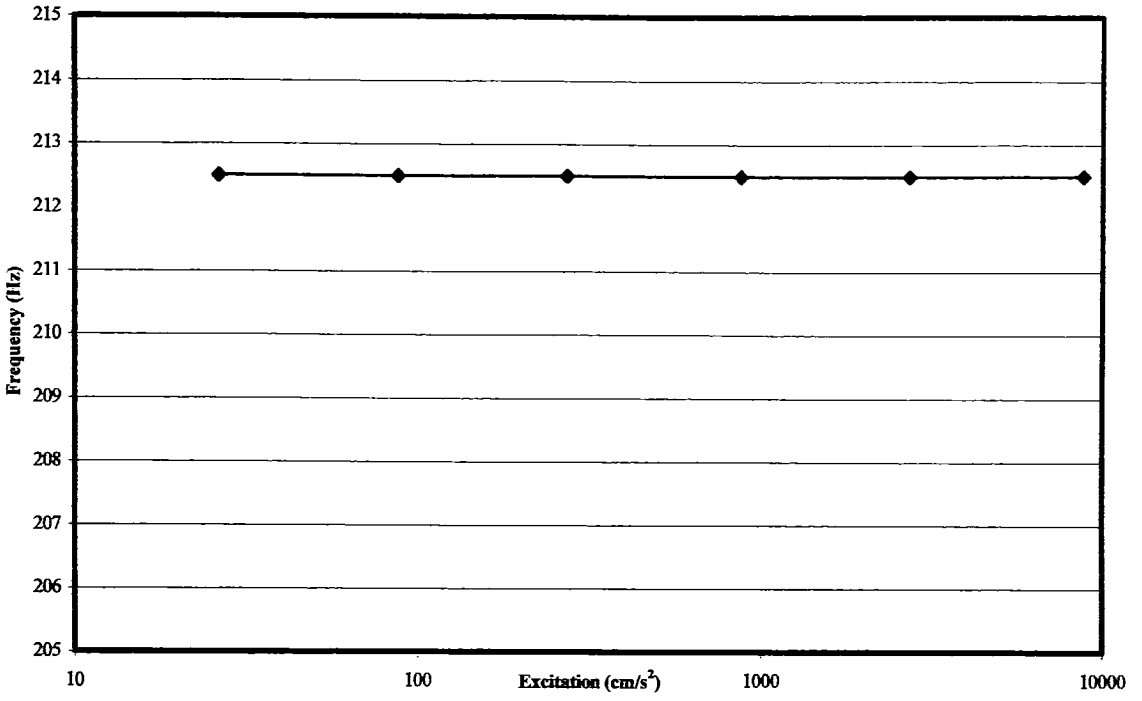

Figure 30 Linearity verification for mode 2 of the untreated beam

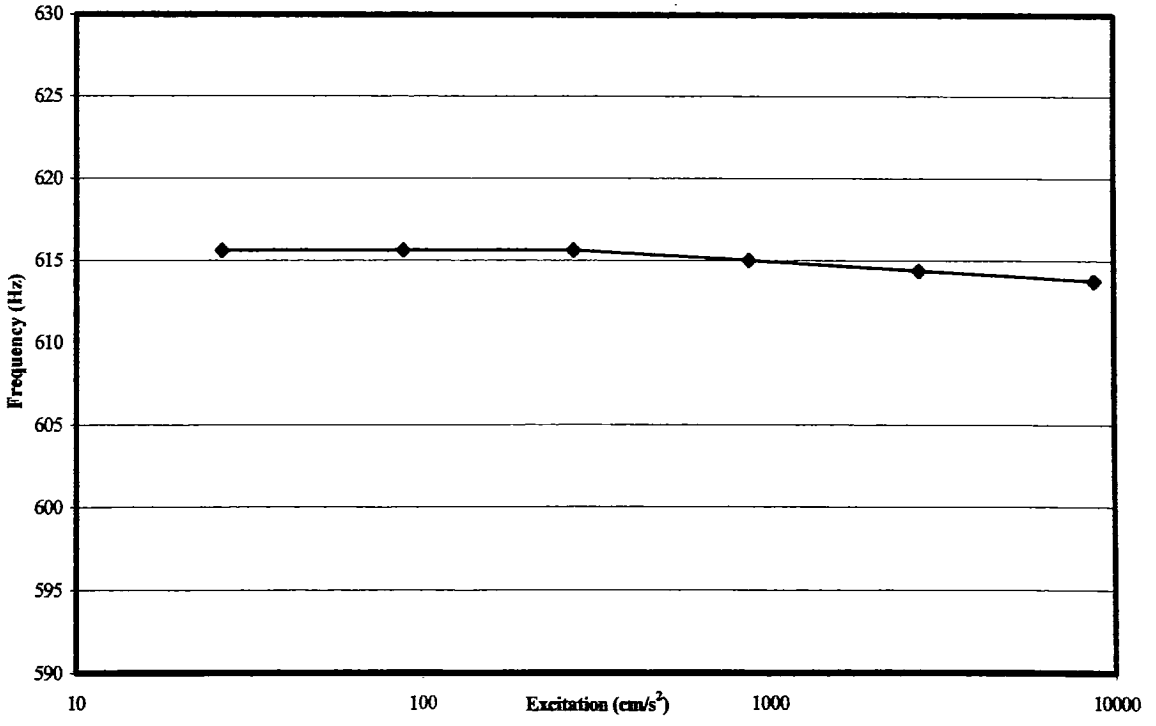

Figure 31 Linearity verification for mode 3 of the untreated beam

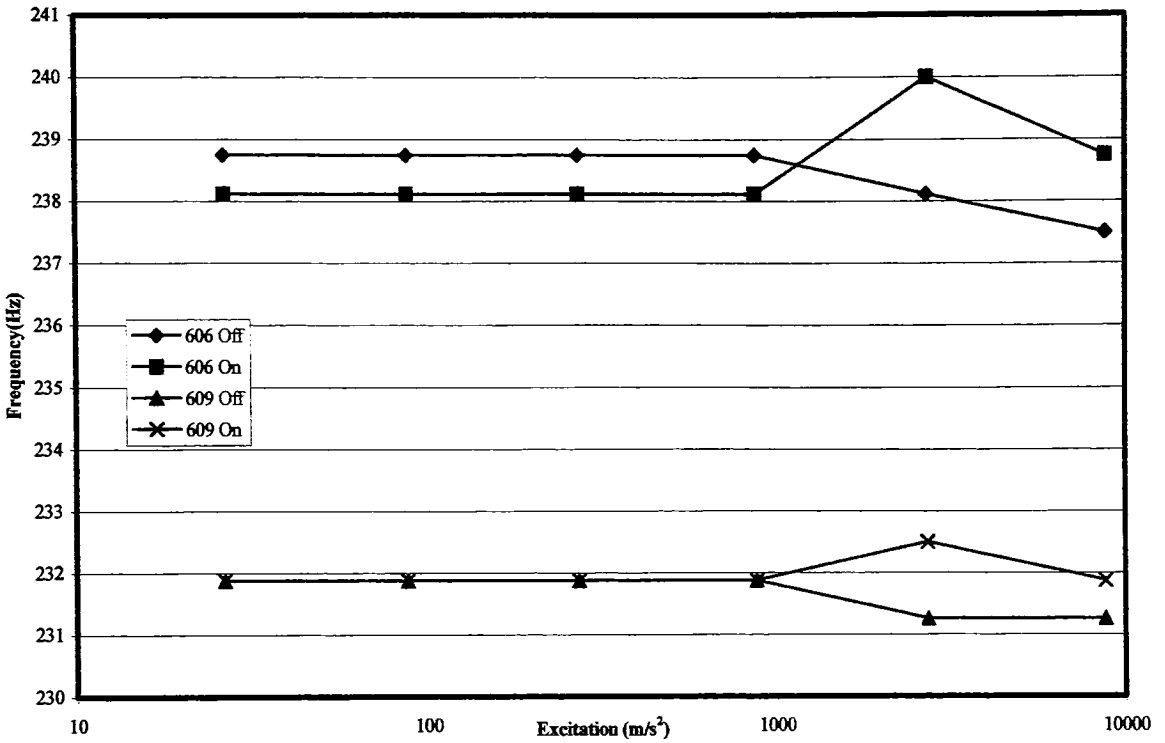

Figure 32 Linearity verification for mode 2 of the treated beams

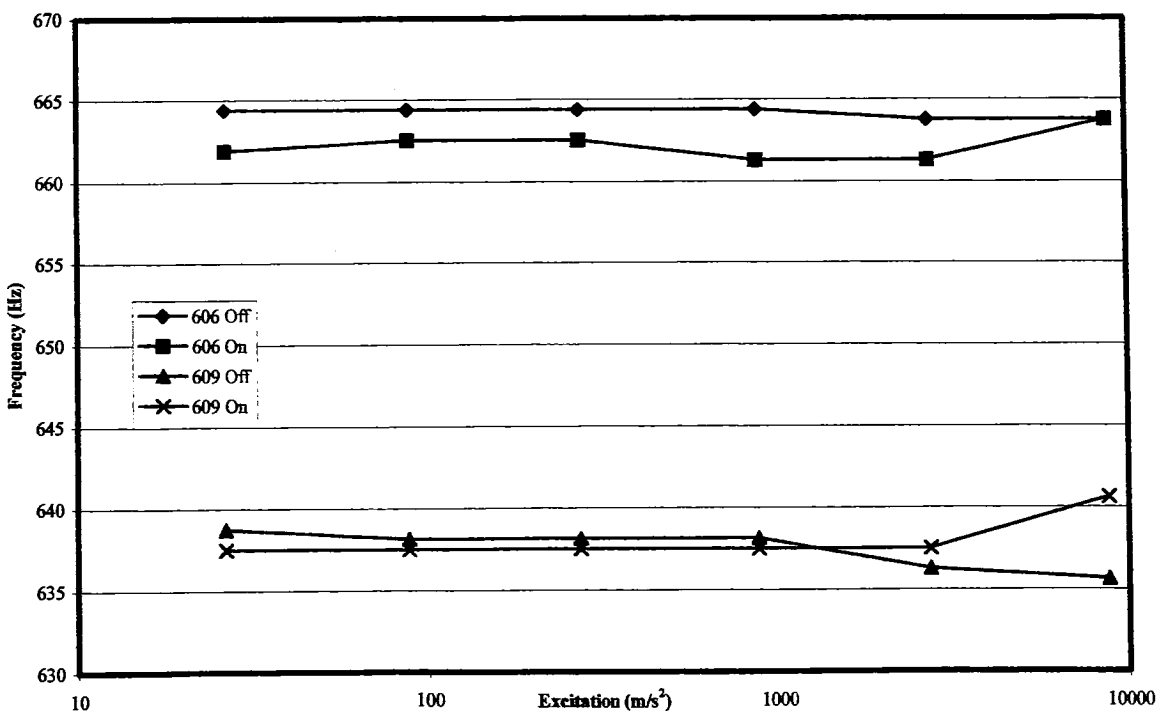

Figure 33 Linearity verification for mode 3 of the treated beams